POLITECNICO DI TORINO

Corso di Laurea Magistrale
in Ingegneria Civile

Tesi di Laurea Magistrale

ECOLOGICAL AND MECHANICAL PROPERTIES OF ULTRA HIGH PERFORMANCE – FIBER REINFORCED CEMENTITIOUS COMPOSITES CONTAINING FLY ASH

Relatore:
prof. Alessandro P. Fantilli

Candidato:
Valerio Lisi

A.A. 2017/2018

Table of Contents

LIST OF FIGURES

The following table shows the list of the figures reported throughout the Thesis.

Chapters 1-4

Annex 1: Geometrical properties

Annex 2: Uniaxial Compression Test

Annex 3: 4 - Point Bending Test

LIST OF TABLES

All the tables reported throughout the Thesis are enumerated in the following list.

Chapters 1-4

Annex 2: Uniaxial Compression Test

Annex 3: 4 - Point Bending Test

Introduction

Use of ultra high performance - fiber reinforced cementitious composite (UHP-FRCC) shows several mechanical advantages. The compressive strength of these composites is higher than 150 MPa. Also, the ductility and the tensile strength is improved by the presence of steel fibers in the mixture. Thus, the UHP-FRCC mixtures appear suitable to reinforce structures, or part of them, made of common building materials. In this work, UHP-FRCC composites are used to reinforce concrete cylinders and mortar beams. The former were reinforced with UHP-FRCC jackets to enhance the compressive strength and ductility of the concrete cores tested under uniaxial compression tests. The latter were strengthened by designing bottom thin UHP-FRCC layers to improve the flexural strength of the beams subjected to 4-point bending tests.

On the other hand, the UHP-FRCC composites have a high ecological impact due to the large amount of cement consumption in the mixtures. The cement production is responsible for large CO_2 quantities released into the environment, due mainly to the calcination of limestone and the high energy consummate during manufacturing. To reduce the ecological impact, two strategies were developed in this study. The "substitution strategy" proposes replacing part of cement mass with fly ash, a waste by-product derived from coal burning. Several studied suggested the addiction of fly ash in the UHP-FRCC mixture to reduce the cement amount, because it releases low quantities of CO_2 and allows creating composites with very dense microstructures. Three mix proportions were implemented considering different cement replacement rates.

The "mechanical performance strategy" suggests the reduction of the UHP-FRCC volume needed for the reinforcement process by enhancing its mechanical efficiency. Improving the mechanical bond between the mortar and the UHP-FRCC layer permitted enhancing the flexural strength of beams subjected to bending load cycles. Different shapes for the UHP-FRCC layers were assessed, designing geometrical wedges on the UHP-FRCC plates or placing steel needles at the contact surface.

The experimental investigations revealed the mechanical benefits due to the UHP-FRCC application, distinguishing the mechanical performances of all the mixtures prepared. These mechanical responses were compared with the ecological impact in order to select the best eco-mechanical solutions among several options. The specimens' comparison was performed using the eco-mechanical chart proposed by Fantilli and Chiaia in [1]. It permitted simultaneously displaying both ecological and mechanical aspects with the aim to tailor eco-friendlier solutions without compromising their mechanical performances. As result, the joint application of both the ecological strategies designed new specimens with lower amount of cement and, at the same time, higher flexural strengths.

Chapter 1

Research Problem and Background

Chapter 1

Research Problem and Background

Ultra high performance – fiber reinforced cementitious composites (UHP-FRCC) show excellent mechanical performances and durability due mainly to the highly dense microstructure and to the presence of steel fibers into the mixture. On the other hand, the sustainability of these cement composites is not always assured because of the high ecological impact depending on the carbon footprint of cement production. Two strategies were described aiming at reducing the effects on the environment. These strategies were applied to decrease the ecological impact of UHP-FRCC reinforcements in concrete cylinders tested under uniaxial compression tests and mortar beams subjected to 4-point bending test. In the first experience, UHP-FRCC jackets were placed around the concrete cores to enhance the compressive strength and the ductility of the cylinders. For the beams, thin UHP-FRCC layers were designed in the bottom part in order to improve the mechanical response to flexural load cycles. An eco-mechanical analysis, based on non-dimensional chart proposed by Fantilli e Chiaia [1], was performed with the aim to select the best ecological solution without compromising the mechanical performance provided by the UHP-FRCC composites.

1.1 UHP-FRCC: High mechanical performances

Ultra-high performance concrete (UHPC) is a particular cementitious composite with a compressive strength higher than 150 MPa [2]. The UHPC mixtures are characterized by the use of a copious amount of cement and a low water/binder ratio. These two aspects lead to a highly dense microstructure, whose porosity results smaller than in normal strength concrete [3]. For this reason, also excellent durability is guaranteed. However, as the material is very compact, it is also very fragile. To overcome this brittle behavior, the addiction of fibers is therefore essential to improve its ductility. As explained in Naaman [4,5], the acronym HPC-FRCC refers to a class of FRCC (Fiber Reinforced Cement Composites) characterized by a strain-hardening behavior in tension after first cracking, accompanied by multiple cracking up to relatively high strain levels (Figure 1.1).
The properly incorporation of steel fibers in UHPC mixture (UHP-FRCC) permits to obtain a material with an ultra-compact matrix (i.e. high compression strength) and, at the same time, higher shear and bending ductility, resistance in tension and energy absorption capacity.

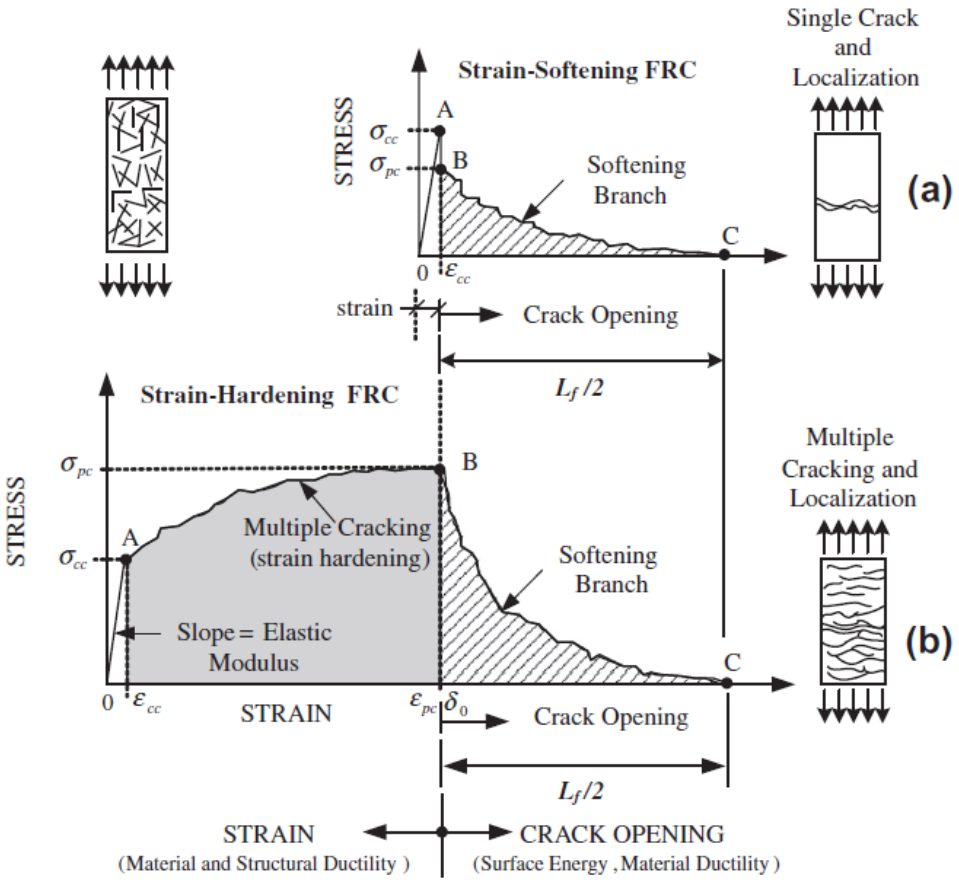

Figure 1.1 – Classification of FRC composites based on tensile behavior [5].

Two main factors allow to UHP-FRCC mixtures achieving high mechanical performances: the highly dense microstructure and the presence of fibers into the blend. The former is mainly responsible for the high compression strength and the high durability, the latter increases the tension resistance, the ductility and the bearing capacity.

As suggested by Bache in his studies on DSP (Densified Small Particles) concrete [6,7], it is possible to increase significantly the strength by using ultra-fine cement particles, as long as the ultra-fine particles could be arranged sufficiently densely and homogeneously. Indeed, the surface forces lock the fine particles in an open structure and, for this reason, the finer the cement, the more difficult the packing. To overcome this problem, these materials are based on very dense and strong binders with 70-80% cement and the remaining 20-30% with micro silica [12]. By using silica as ultra fine particles, it is possible to create dense and homogeneous granular matrix because micro silica is less reactive than cement. As shown in Figure 1.2.a adapted from [8], the structure of strong binder material is composed of densely packed cement and ultrafine spherical silica particles arranged homogeneously in the spaces between the cement particles.

Therefore, the use of silica particles in the binders permits to obtain denser microstructure with low porosity and consequently materials with higher compression strength [9].

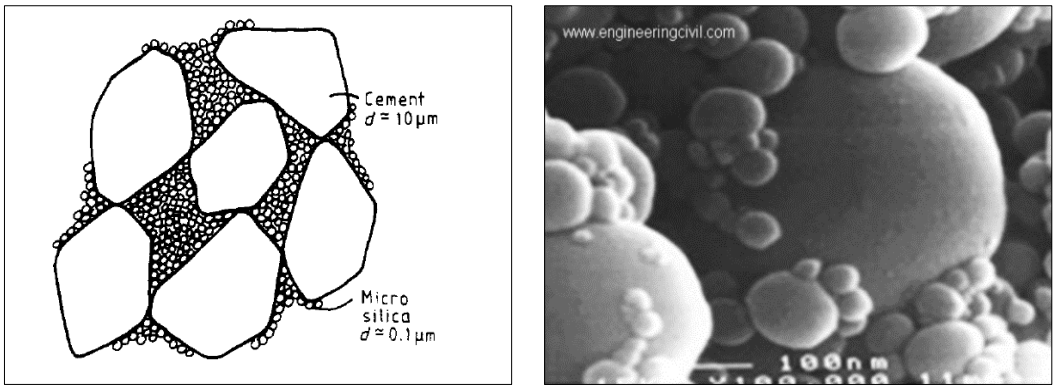

a) b)

Figure 1.2 – The densely microstructure of strong binders composed of cement and silica particles: a) Ultrafine spherical silica around cement (picture adapted from [8]); b) image obtained by SEM (from [33]).

A characteristic limitation of most of these strong materials based on highly dense microstructure is their extreme brittleness. Therefore, the addiction of fibres in the mixtures results essential to improve their ductility. The addiction of fibers to DSP matrices leads to Ultra-High Performance Fibre Reinforced Concrete (UHPFRC). As explained in Rossi [10,11], the effect of fibres concerns both material and structure behavior.

For a better understanding these concepts, the Author proposed some definitions [12]:

- "*microcrack* is a crack whose length can be considered to be very small in relation to the size of a specimen or a structure";
- "*macrocrack* is a crack whose length cannot be considered to be very small in relation to the size of a specimen or a structure";
- "*active crack* is a crack whose edges undergo normal or tangential displacements";
- "*critical and active crack* is a crack which leads to a concentration of stresses and a localization of strains within a volume of concrete".

In this way, we can describe the transition from the material behavior to the structure behavior as the transition from active microcracking to active macrocracking. The fibers have a two-fold role during the cracking process. Initially, during the phase of random microcracking, they permit to spread active cracks and to delay their localization. This allows to reach higher strength and ductility at material scale. When the macrocracks become active and try to propagate, the metal fibers can also prevent the cracks localization providing higher bearing capacity and ductility at

the scale of structure. In a general sense, short fibers are mainly required to act on microcracks, whereas long fibers affect mostly on macrocracks ([13]). In figure 1.3 it is illustrated the role played by the micro and the macro fibers during cracking process of a FRCC subjected to tensile stress [14].

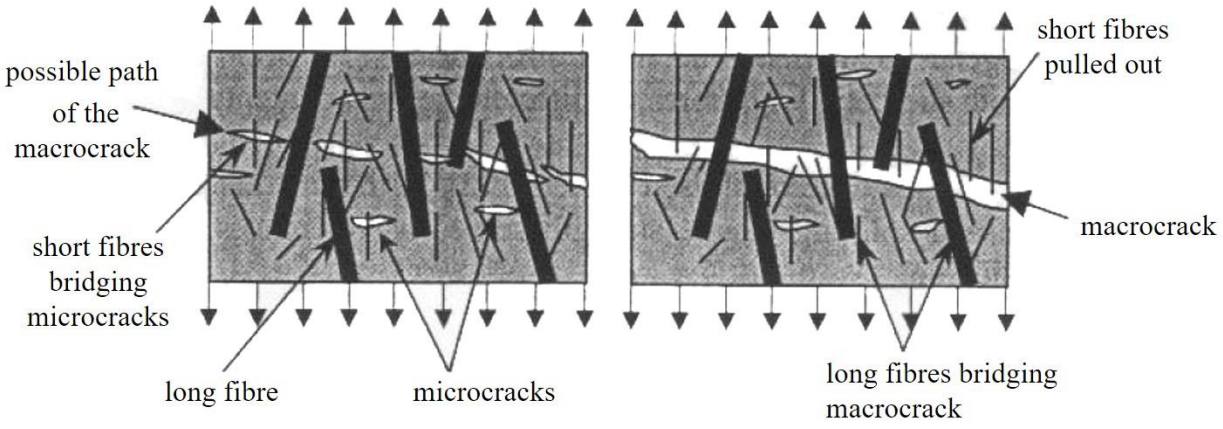

Figure 1.3 – Action of the different fiber types in FRCC (Markovic et al. [14]): short fibers bridge the microcracks before and at the peak stress; long fibers bridge localized macrocracks in the softening stage. Pictures adapted from [13].

Also, it is possible to distinguish the effect of fibers in tension and in compression. In the first case, high proportion of short fibers enhances tensile strength and ductility at the material scale, while the addiction of low percentages of long fibers permits to increase the ductility at structure scale. Furthermore, the compressive strength results less influenced by the amount of short fibers, while the bearing capacity and the ductility at structural scale is still improved by the long fibers.

Thus, the main advantage of using fibers in UHP-FRCC mixtures is to improve the mechanical performance under tensile stress (increment in strength and ductility) and to maintain also a good ductility in compression. With regards to compressive strength, most part of the mechanical improvement is due to the compactness and the highly dense microstructure of the matrix. It is achieved by using very low water-cement ratios with high cement content. This is the main cause of high ecological impact showed by UHP-FRCC composites. The cement manufacturing, as described in the next section 1.2, is responsible of high CO_2 amount released in the environmental. For this reason, in this work (see section 1.3), different strategies were implemented to reduce the cement content and the ecological impact of UHP-FRCC mixtures but, trying to preserve the mechanical performances provided by this high strength material.

1.2 UHP-FRCC: High Ecological Impact

According to the estimates made by Brand et al. in [15,16], the industrial sector is responsible approximately for a quarter of global carbon dioxide (CO_2) emissions. In these reports, the CO_2 emissions from cement plants represents no less than 5% of total anthropogenic emissions. Other studies on the Life Cycle Assessment (LCA) for concrete structures attributes the 85% of CO_2 emissions to cement production [17]. The 95% of the CO_2 is produced during the cement fabrication, while the remainder 5% is connected to the transportation of raw materials and finished products [18]. The ecological impact of cementitious composites mainly depends on the carbon footprint of cement manufacturing. Indeed, the clinker, which is the main material used all over the world to produce cement, releases a bit less than 1 ton of CO_2 per ton of clinker produced [19].

Considering Ordinary Portland Cement (OPC), traditionally binder used for concrete, the causes of high CO_2 emissions are mainly the calcination of limestone and the high energy consummate during manufacturing. According to Turner and Collis [20], the carbon footprint assessment should also consider the energy consumption for activities associated with the concrete production, as mining and transport of raw materials, manufacturing and construction procedures. Therefore, in this work, the high amount of cement used for UHPC is considered responsible for the high impact on the environment. The functional unit, considered for the ecological performances analysis, was defined as the amount of CO_2 emitted during all the activities necessary to produce 1 m^3 of UHP-FRCC (Figure 1.4). It also includes the CO_2 emission due to the steam curing process, regarded as 120 kg/m^3 in accordance with the already mentioned Turner and Collins' study.

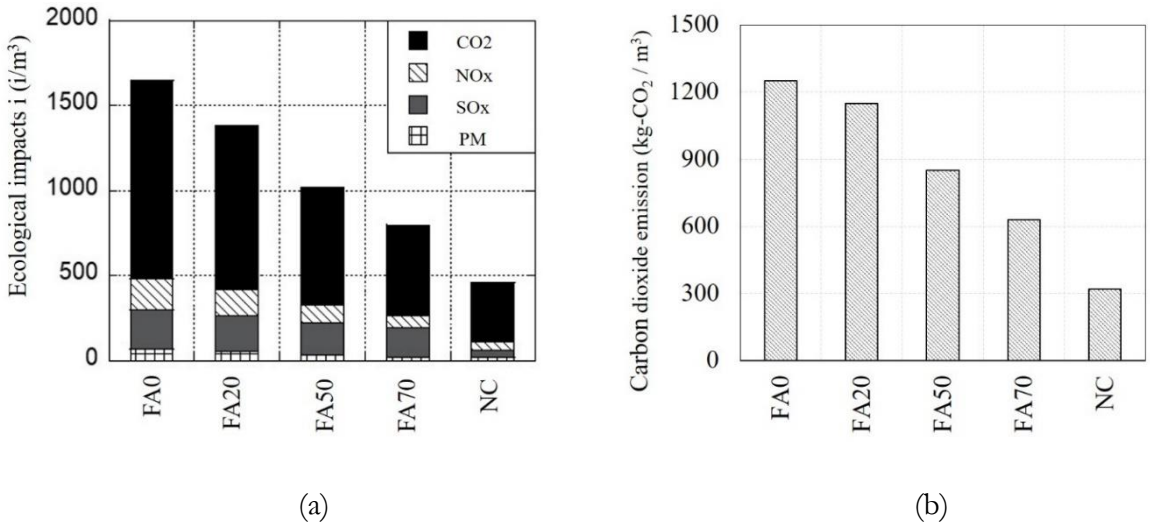

Figure 1.4 – The impact of a cubic meter of UHP-FRCC, in terms of (a) greenhouse gases emission, and (b) carbon footprint. Pictures adapted from [27].

1.3 Carbon mitigation strategies

As explained in the previous section, the impact of cement manufacturing on the environment is very high. To reduce this ecological impact, two main strategies are developed in this study.

The former, named "material substitution strategy", already presented in Habert and Roussel's work [19], consists in partially replace of cement amount. During the experimental investigation, we considered different mixtures in which part of cement was substituted with fly ash (Figure 1.4.a). Fly ash is a waste by-product derived from coal burning. As described in [20] and [21], it releases low quantities of the CO_2. Thus, replacing part of the cement content with fly ash could be an effective way to improve also the ecological properties of UHP-FRCC.

When the content of fly ash is above the 50% by mass of the total cementitious materials, concrete is generally defined as High Volume Fly Ash (HVFA) [22]. In general, HVFA concrete posses excellent cohesivness and workability. This characteristic makes HVFA suitable to pumpatibility and compactibility. The fly ash particles, as illustrated in Figure 1.5.c, are finer and more spherical than Portland cements ones. It allows to create a very dense microstructure with low porosity, thereby excellent durability [23]. HVFA concrete shows low water permeability, high resistance to freezing and thawing cycling, great opposition to chloride ion penetration and good resistance to sulphate attack and to carbonation [24].

(a)

(b)

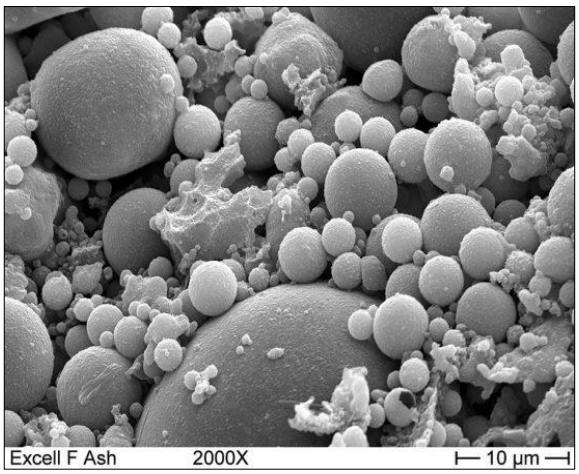

(c)

Figure 1.5 – "Substitution strategy" consists in replace part of cement with fly ash: a) cement and fly ash powders comparison; b) fly ash powder (naked-eye view); c) fly ash particles are finer and more spherical than Portland cement (microscope view). Picture a) adapted from [34], Pictures b) and c) adapted from [35].

Different UHP-FRCC mixtures were prepared increasing the amount of cement replaced by fly ash. No substitutions were considered for FA0 mixture, while for FA20 and FA70, the percentage (in weight) of cement replaced where, respectively, 20% and 70%. As proposed in Table 1.1 for FA70 mixture, replace part of cement content in FA0 with fly ash has permitted to obtain the same total cement volume ratio present into an ordinary concrete mix proportion.

Table 1.1 – Mix proportion comparison (volume ratio).

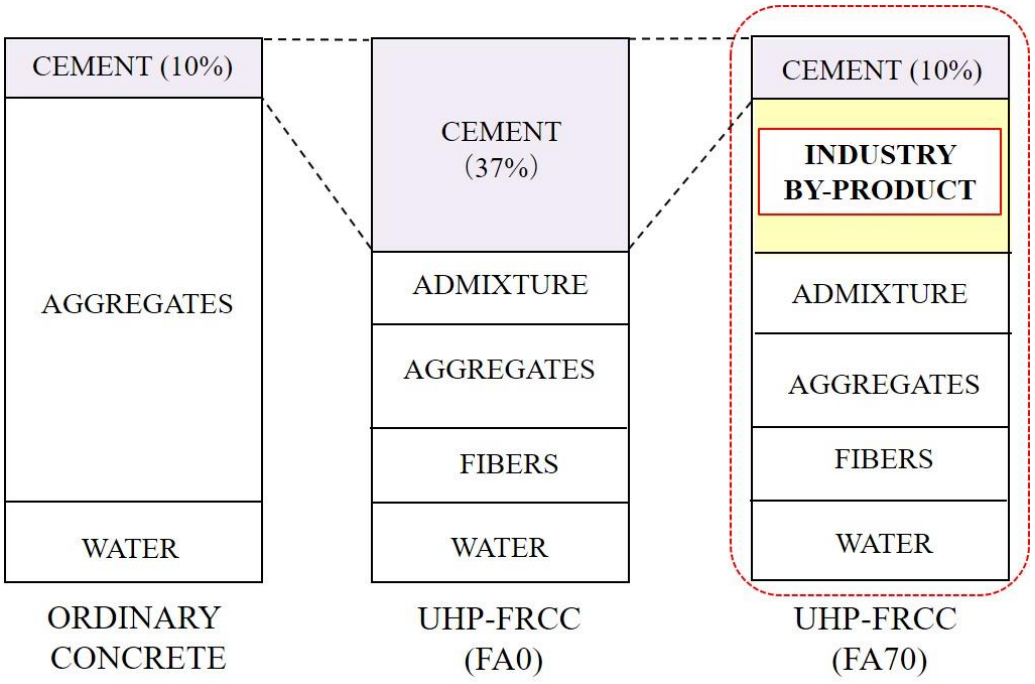

It must be remarked that the substitution of cement with HVFA is not always convenient. Indeed, even if HVFA leads to benefit on environmental impact, it also reduces the UHP-FRCC strength, especially at early age [25].

Recently, Aghdasi et al. [26] used a large amount of fly ash in UHP-FRCC, but to replace sand, instead cement, and increase the flowability in large scale casting. Such cement-based composites showed that benefits on the environments, achieved with the substitution of high volume of cement with fly ashes, are paid in terms of compressive strength, which not always remains higher than 150 MPa. In other words, the substitution strategy often compromised the mechanical performances provided by UHP-FRCC. For these reasons, the replacement of cement with fly ash should be tailored by balancing both mechanical and ecological performances. To do this, the eco-mechanical analysis, based on the non-dimensional chart described in section 1.4, were performed and their results were discussed in the following Chapters.

The second strategy implemented to reduce the ecological impact of UHP-FRCC reinforcement was the "mechanical performance strategy". This strategy, inspired by the "material performance strategy" presented in Habert and Roussel's work [19], suggests the reduction of the UHP-FRCC volume needed for reinforcement process by enhancing its mechanical performances.
During the second experimental campaign, in which mortar beams were reinforced with thin UHP-FRCC layers, different solutions were proposed to improve the mechanical bond between mortar and UHP-FRCC (Figure 1.6).

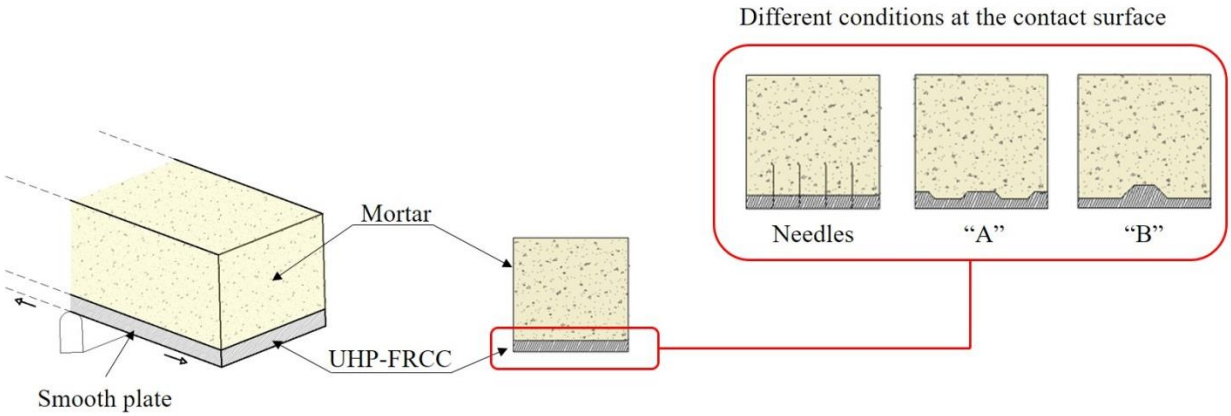

Figure 1.6 – Application of "mechanical performance strategy": increasing the grip condition leads to higher resistance. As result, it is possible to achieve the same mechanical performances using lower UHP-FRCC content.

Using steel needles or varying the geometry of the thin layer, it was possible to achieve a higher flexural strength without changing the amount of UHP-FRCC used. Proper design of the boundary condition allows to obtain beams with unified behavior between mortar and UHP-FRCC. Thus, through an accurate study of the boundary condition, it was possible to achieve the same mechanical performances reducing the amount of UHP-FRCC used as reinforcement.
Different solutions were designed to increase the effectiveness of the reinforcement: steel needles were included between the mortar and UHP-FRCC contact surface and two geometrical shapes were designed for the UHP-FRCC layer. The casting procedures for each type of UHP-FRCC layer are shown in Chapter 2, where the experimental investigation is illustrated.

1.4 Eco-mechanical analysis

With the aim to select, or tailor, an eco-friendlier solution without compromising the high performance ensured by UHP-FRCC use, an eco-mechanical analysis was performed through the non-dimensional diagram proposed by Fantilli and Chiaia [1]. On the horizontal axis of this diagram (Figure 1.7), the mechanical response is described by the Mechanical Index (MI), where MI_{inf} is the lower bound value of the mechanical performances. Furthermore, the ecological performances are reported on the vertical axis, defined by the Ecological Index (EI), whereas the upper bound value of ecological impact is represented by EI_{sup}.

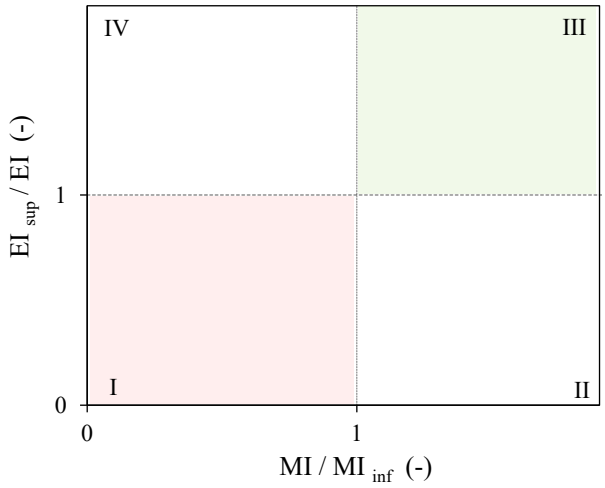

Figure 1.7 – The non-dimensional chart for assessing the eco-mechanical performances based on [1].

Accordingly, four different zones can be detected within the non-dimensional diagram:

- Zone I: Low mechanical performances – Low ecological performances;
- Zone II: High mechanical performances – Low ecological performances;
- Zone III: High mechanical performances – High ecological performances;
- Zone IV: Low mechanical performances – High ecological performances.

The study aims to select the best solutions among those falling within the third region (depicted in green). To describe the mechanical performances, different mechanical parameters were considered according to the test performed (max compressive stress, max flexural strength). For the ecological performances, always the mass of CO_2 released by the production of 1 m^3 of UHP-FRCC was considered as an environmental marker.

Finally, it's important to point out that changes in the chart bounds (MI_{inf} and EI_{sup}) lead to different eco-mechanical results. Indeed, different assessments were carried out by varying the referencing performance. Examples of application were shown in Chapter 3.

1.5 Research significance

The goal of this study is to present some advantages in the use of ultra-high performance fiber reinforced cementitious composite (UHP-FRCC) as reinforcement for elements made of common building materials, such as concrete and mortar.

As suggested by Naaman [4], only a selected zone of the structure may be in need of strengthening or toughening. To reinforce these zones, the use of UHP-FRCC is often competitive and economically justifiable. On the other hand, as illustrated in the previous sections, the copious amount of cement used in the mixture causes a high environmental impact. For this reason, necessary efforts in term of ecological impact reduction have to be made. Two strategies were proposed to reduce the ecological influence of UHP-FRCC reinforcement. The "substitution strategy" proposes to replace part of cement with fly ash, an eco-friendlier by-product derived from the coal burning. The "mechanical performance strategy", instead, suggest enhancing the mechanical efficiency of the reinforcement so that reduce its amount. Indeed, even if the same quantity of UHP-FRCC is used as reinforcement, better mechanical bond at contact surface allows to take full advantage of UHP-FRCC properties.

Both the two experimental investigations carried out for two different types of samples and using different testing modalities, show the mechanical advantages of UHP-FRCC use. But, if for the first experience (i.e., concrete cores reinforced by UHP-FRCC jackets) the eco-mechanical analysis showed the mechanical ineffectiveness of the "substitution strategy", in the second experience the joint use of both the strategies allowed to obtain higher mechanical and ecological performances. For these reasons, the aim of the work is to present the mechanical benefits due to the UHP-FRCC reinforcements, but at the same time to suggest a proper way to apply the ecological strategies above described.

Figure 1.8 – Central Avenue Villas, an award-winning eco-friendly condominium complex in Oklahoma City, also used a combination of fly ash concrete and ICF (Insulating Concrete Forms) to form the interior and exterior walls. Picture adapted from [35].

1.6 Thesis organization

This Thesis work is organized in 4 main Chapters. The introduction and the discussion about the state of the art is shown in Chapter 1. It describes also the mechanical and ecological performances provided by the UHP-FRCC composites, and it illustrated the non-dimensional chart proposed to perform the eco-mechanical comparison between the tests results. All the aspects connected to the experimental campaign are reported in Chapter 2. This Chapter is divided in two main sections: the first part is based on the concrete cores reinforced with the UHP-FRCC jackets; the second part mostly concerns the investigation on mortar beams subjected to flexural load and reinforced by thin UHP-FRCC bottom layers. For each type of specimen first the material specifications are pointed out, then the casting and curing procedures are illustrated. Finally, all the experimental devices and the test method are detailed. The Chapter 3 shows the results obtained during the experimental investigation. At the beginning, the mechanical parameters are illustrated comparing the performances provided by the different UHP-FRCC mixtures. Then, the eco-mechanical analysis is performed focusing on a single case to better understand the procedure. All the results are shown together in a final comparison chart, where both mechanical and ecological performances provided by all the samples are analyzed.
At the end, Chapter 4 contains the conclusions and the future research developments. The entire Thesis work is retraced focusing on the key points faced along the way. The experimental results were remarked underlining the innovative aspects of the study and suggesting some potential future options. Lastly, all the graphs, tables and figures not mentioned in the body of the Thesis, but still important to understand the complete work, are shown in the Annexes.
The Annex 1, describes the geometrical properties of all the samples made and tested during the experimental campaign. All the compressive stress-strain curves and the mechanical parameters concerning the concrete cores confined by UHP-FRCC jackets are depicted in the Annex 2. The Annex 3 contains the bending moment-curvature curves of all the beams tested under flexural load cycles.

Chapter 2

Experimental Investigations

Chapter 2

Experimental Investigations

Two main typologies of specimens have been designed and tested in the "Life Cycle Engineering Laboratory of Tohoku University". The first type considered concrete cylinders reinforced with UHP-FRCC jackets and tested under uniaxial compression. During the work, following the "material substitution strategy", different specimens were prepared to change the jacket's mix proportion. The first series was realized with UHP-FRCC considering no fly ash substitution (FA0). In the second and third series, the replacements rates of cement with fly ash were, respectively, 20% (FA20) and 70% (FA70). The second experiment instead, included mortar beams reinforced with UHP-FRCC thin bottom layer subjected to a 4-point bending test. In the first series, these reinforce layers were realized with UHP-FRCC without fly ash content and, according to the "mechanical performance strategy", different solutions were proposed to enhance the efficiency of the reinforcement. Lastly, as done for the first type of experiments, in the successive series different UHP-FRCC mixtures were prepared and their performances compared.

2.1 Concrete cylinders reinforced with UHP-FRCC jackets

2.1.1 Geometrical Properties

Concrete cylinders (NC) with 50 mm radius and 200 mm length were cast following the mix proportion showed in Table 2.2. The UHP-FRCC jackets were designed with a length L_j lower than the concrete core's height L ($Lj < L$). This choice permitted to consider the jacket's effect only as confinement effect on the cores and with no directly contribute to compression. Geometrical characteristics of the specimens realized are shown in Figure 2.1 and Table 2.1.

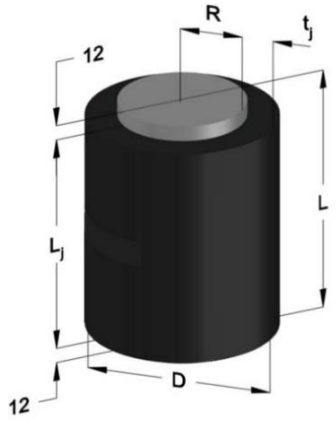

Figure 2.1 – Concrete core reinforced with UHP-FRCC jacket.

Table 2.1 – Geometrical properties of specimens.

R (mm)	L (mm)	tj (mm)	Lj (mm)	D (mm)
50	200	25	176	150

Note: R: Core radius; L: Core height; tj: jacket's thickness; Lj: jacket's height; D: total diameter.

2.1.2 Material specifications

The concrete cores were cast using High Early Strength Portland Cement (HESP Cement), water (W), fine aggregates (Sand) with diameters less than 5 mm and coarse aggregate (Coarse), which size was between 5-20 mm. To improve the workability, also superplasticizer (SP) was added to the mixture. The mix proportion for the concrete cores is illustrated in Table 2.2.

Table 2.2 – Mix proportions of concrete cylinders.

	HESP Cement (kg/m^3)	Sand (kg/m^3)	Coarse (kg/m^3)	W (kg/m^3)	SP (kg/m^3)
CONCRETE CORES	300.3	836.0	900.3	171.7	1.7

Note: B: binder; HESP Cement: High Early Strength Cement; Sand: fine aggregate; Coarse: Coarse aggregate; W: water; SP: superplasticizer.

Three different series of UHP-FRCC jackets were made according to the mix proportions shown in Table 2.3. Low heat cement (LH Cement), silica fume (SF) and fly ash (FA) were used as the binder. Also, Silica sand (S) and wollastonite fibers (Wo) were used. In the Water (W), superplasticizer (SP) and defoaming agent (DA) were diluted. All the mixtures were fiber-reinforced with 1% of volume of steel micro-fibers (named OL, see Figure 2.2.a) and 1.5% in volume of steel macro-fibers (named HDR, see Figure 2.2.b), whose properties are reported in Table 2.4.

Table 2.3 – Mix proportions (wt.%) of the UHP-FRCC.

Series	Binder (B)			S / B (%)	Wo / B (%)	W / B (%)	SP / B (%)	DA / B (%)
	LH Cement / B (%)	FA / B (%)	SF / B (%)					
FA0	82	0	18	35	13	13.8	2.2	0.02
FA20	65.6	16.4						
FA70	24.6	57.4						

Note: B: binder; LH Cement: Low Heat Cement; FA: fly ash; SF: silica fume; S: aggregate; Wo: wollastonite; W: water; SP: Superplasticizer; D: defoaming agent.

Table 2.4 – Steel fiber characteristics.

Steel fibers	Density (kg/m^3)	Length (mm)	Diameter (mm)	Tensile strength (MPa)	Aspect ratio (-)
OL (Micro)	7850	6	0.16	2000	37.5
HDR (Macro)	7850	30	0.38	3000	78.9

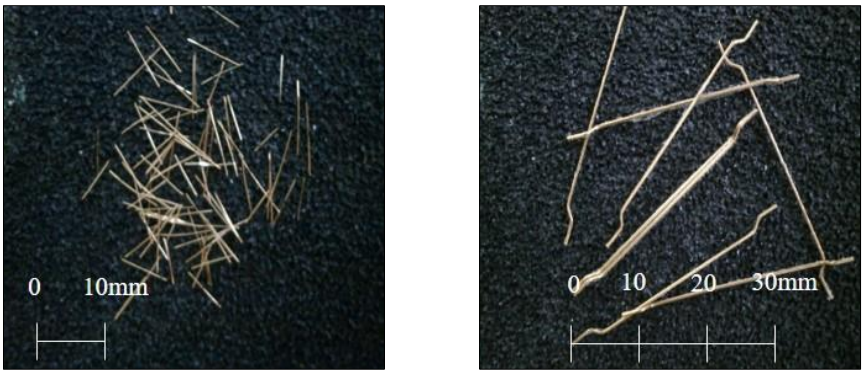

(a) (b)

Figure 2.2 – Steel fibers added to the mixture: a) OL; b) HDR.

Cylinders, with 50mm radius and 100 mm in height, were tested by uniaxial compression to measure the mechanical properties of all the materials used in the experiments. The results are shown in Table 2.5.

Table 2.5 – Results of uniaxial compression on cylinders (R=25 mm, h=100 mm).

TYPE	Compressive strength (MPa)	Young's Modulus (GPa)
CONCRETE (SERIES 1)	45.1	34.6
CONCRETE (SERIES 2)	45.0	34.6
UHP-FRCC FA0	204.7	54.4
UHP-FRCC FA20	193.4	53.5
UHP-FRCC FA70	150.7	49.6

2.1.2 Casting and curing procedures

Wooden rings, with 12 mm in height and inner radius equal to the cores' radius R, were used at the base of the jacket's mold. Paper cylinders, with 150 mm diameter and 178 mm height, were used to cast the UHP-FRCC jackets around the cores, as shown in Figure 2.3.

Figure 2.3 – Paper mold used for the jacket casting and the final specimen obtained.

For the first series, 5 concrete cores were cast. Embedded strain gauges were installed as described in the following section. As illustrated in Figure 2.4, the specimens were left for 48 hours in the molds at the temperature of 20 °C and 95% *RH*, then the formworks were removed. After 11 days from the cast, 3 of them were reinforced with the jackets, realized with no substitution of fly ash (FA0 mixture) and the others were left with no reinforcements. Two days later, also the jacket's formworks were removed, and all the specimens were subjected to steam curing for the following 48 hours. Finally, all the samples were stored in the same humidified environment (20 °C and 95 *RH*) until the test day, performed the 28th day after cores cast.

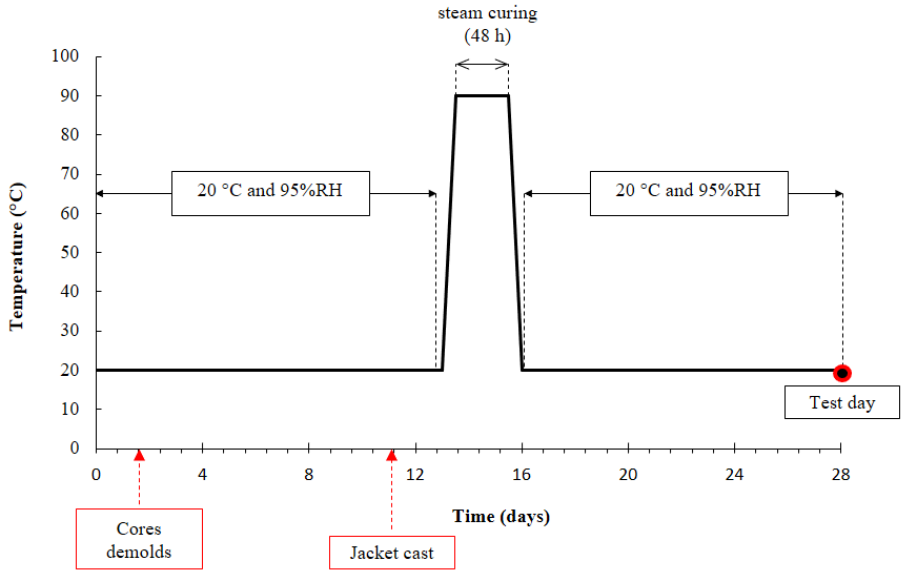

Figure 2.4 – Curing procedure for confined specimens.

For the second series, 8 concrete cores were cast. Following the same procedure described below, after 11 days from the initial cast, 6 specimens were reinforced with the UHP-FRCC jackets, and 2 specimens were left without jackets. Three of these jackets were realized with a mixture having 20% replacing of cement with fly ash (FA20 mixture) and the other three with 70% of substitution (FA70 mixture). The same curing procedure, above mentioned, was carried out, and the test was performed after 28 days from the concrete cast. At the end of every cast, mixture fresh properties were measured considering the flow table-test and the air content test.

Figure 2.5 – UHP-FRCC cast phases (FA0 mixture).

To assess the fresh concrete consistency, defined as the ability of concrete to flow, the slump flow test was performed according to ASTM C 143/C 143M – 03 [42]. The test is carried out using a metal mold in the shape of a cone, known as a slump cone or Abrams cone, that is open at both ends and has an attached handle (Figure 2.6.a). The tool, typically, has an internal diameter 100 mm (± 2mm) at the top and 200 mm (± 2mm) at the bottom with a height of 300 mm (± 2mm). This cone is placed on a non-absorbent (rigid) surface. It shall be held firmly in place during filling by the operator standing on the two-foot pieces. It is immediately filled with fresh concrete in three layers, each approximately one third the volume of the mold. Each time, each layer is tamped 25 times with a 600 mm long bullet-nosed metal rod measuring 16 mm in diameter. For the bottom layer, it is necessary to incline the rod slightly and to make approximately half of the strokes around the lateral perimeter, and then progressing with vertical strokes spirally toward the center. For the second layer and the top layer, the strokes should just to penetrate the layer avoiding compacting also the underlying stratum. When also the top layer has been rodded, with a rolling motion of the tamping rod the exceeding concrete should be removed. Then, the mold is removed from the concrete by raising it carefully in vertical direction. Immediately the slump is measured by determining the vertical difference between the top of the mold and the displaced original center of the top surface of the specimen (Figure 2.6.b).

(a) (b)

Figure 2.6 – Slump flow test used for the concrete (cylinders): a) Abrams cone; b) assessment of slump value [36].

The flow of hydraulic cement mortars was determined according to ASTM C1437 – 07 [43]. The flow table and the flow mold considered for the test were conforming to ASTM C230 - 08 [44] (Figure 2.7.a). After cleaning and drying the flow table's surface, the flow mold was placed at the center and was filled with 3 layers of mortar. Each layer, with about 25 mm in thickness, was tamped 20 times with a tamper conforming to the requirements of ASTM C109/C 109M [45].

The exceeding mortar from the top layer were cut off and the table were carefully cleaned and dried with particular attention paid to remove any water from around the edge of the flow mold. The mold was lifted away from the mortar and the table were dropped 25 times in 15 seconds. To assess the flow of spread mortar, the diameter, along 4 lines on the table top, were calculated (Figure 2.7.b). The flow indicates the workability of the mortar. The initial and final diameters of the mortar samples are used to calculate the flow. The flow is defined as the increase in diameter divided by the original diameter multiplied by 100.

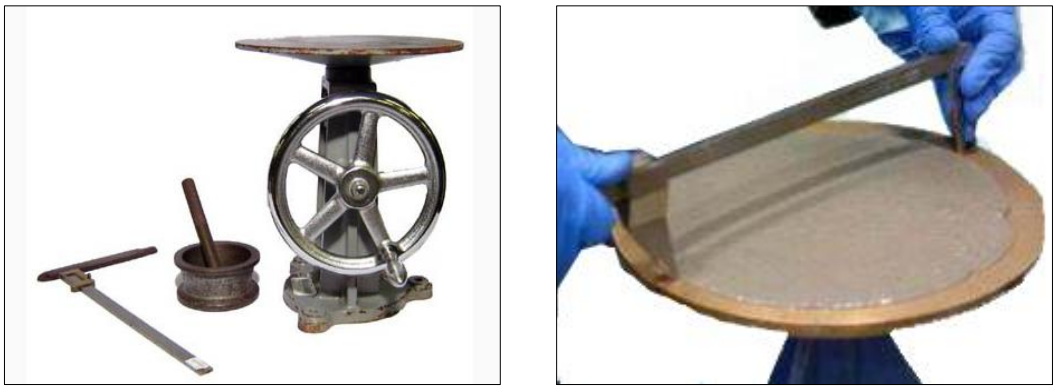

(a) (b)

Figure 2.7 - Flow test used for the mortar (beams): a) flow table [37]; b) diameter measurement on spread mortar [38].

The air content of freshly mixed concrete was measured according to ASTM C231 – 03 [46] using the Pressure Method. This method covers the determination of the air content from observation of the change in volume of concrete with a change in pressure. During the test, a Meter Type "B", consisting of a measuring bowl and a cover assembly (Figure 2.8.a), was filled with fresh concrete in 3 layers. The first layer was tamped 25 times throughout its depth with the rod and 15 times on the lateral side of the bowl using the mallet. This procedure was repeated for all the 3 layers. To striking off the exceeding concrete from the top layer, the upper surface was pressed with a plate with a sawing motion to produce a smooth finish (Figure 2.8.b). After properly cleaning the bowl edge, the cover was assembled, and the main air valve was closed while the petcocks were opened. Then, the main bleeder valve was closed, and the dial was pumped till the initial pressure. Once stabilizing the gauge by hand, the main air valve was reopened, the pressure was released and the Apparent air content (A_1) was read on the display. The correct air content of the sample tested (As) was calculated from A_1 by subtracting the Aggregate Correction Factor (G), according to:

$$A_s = A_1 - G$$

(a) (b)

Figure 2.8 – Air content measured by the Pressure Method: a) Air Meter Type "B" [39]; b) smooth top surface.

2.1.3 Experimental devices and Test Method

The uniaxial compression test was performed under deformation control. To record the strain, the following devices were used during the experiments:

- Compressometer (Figure 2.9.a);
- Strain gauges (Figure 2.9.b);
- Embedded strain gauges (Figure 2.9.c).

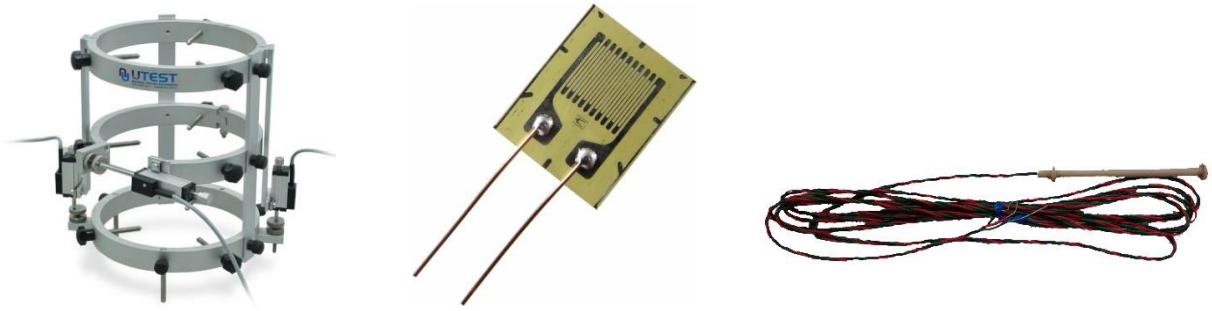

(a) (b) (c)

Figure 2.9 – a) Compressometer [40]; b) Standard strain gauge [41]; c) Embedded strain gauge.

The Compressometer is used for evaluating deformation and strain characteristics of concrete cylinders under compression test (Figure 2.10.a). In this work, it was applied to the concrete cores without jackets to record their characteristic stress-strain curve. Using these data, the load peak and the maximum strain were calculated in order to define the Young's modulus of the concrete cores without confinement effects.

Strain gauges are electrical sensors used for the measurement of strain. They are designed to convert mechanical motion into an electronic signal. A change in resistance is proportional to the strain experienced by the sensor and, for this reason, measuring this electrical signal permits to obtain the strain. Four strain gauges were put on each jacket's surface: two placed in vertical direction and two on horizontal direction. The vertical ones measured the strain along the axial axis, the others recorded the transversal dilatation (Figure 2.10.b).

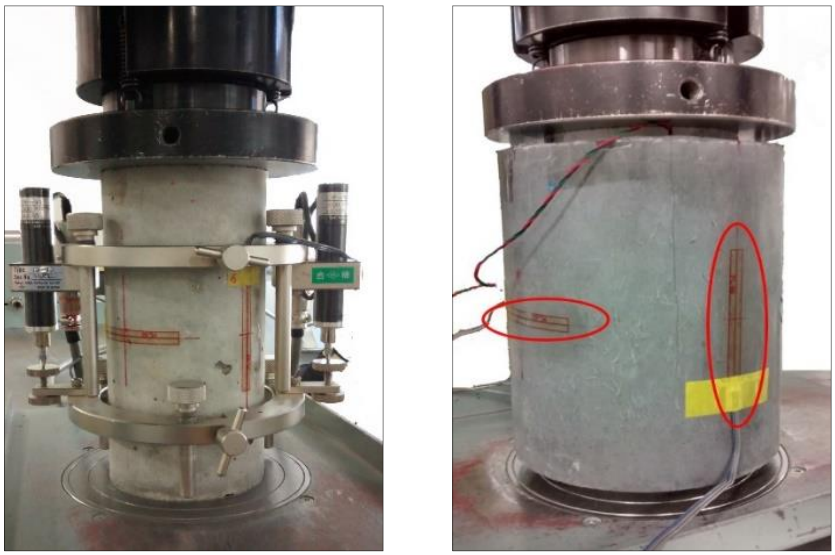

(a) (b)

Figure 2.10 - Deflection measurement:
a) Compressometer on concrete core; b) Strain gauges applied on the jacket's surface.

As shown in previous experiences [28], the vertical strain gauges applied directly on the jacket's surface are not suitable for detecting the vertical strain. Indeed, use of these strain gauges on the jacket surface leads to measure negative values for deformation (i.e., elongation) due to the bending effect on the jacket (see Figure 2.11.a where it is depicted the strain measured by vertical strain gauges on a cylinder confined with a FA20 jacket). When the load is applied only on the core part, the outermost part of the jacket's surface starts to dilate assuming a trapezoidal shape (Figure 2.11.b). On the other hand, the concrete cores subjected to the uniaxial compression load are crushed and the deformation should be positive (i.e., compression). For this reason, the strain values measured by the two vertical strain gauges placed on the UHP-FRCC jacket's surface did not portrayed the real condition of the concrete cores and they could not be used to describe the compressive stress-strain relationship of the confined cylinders.

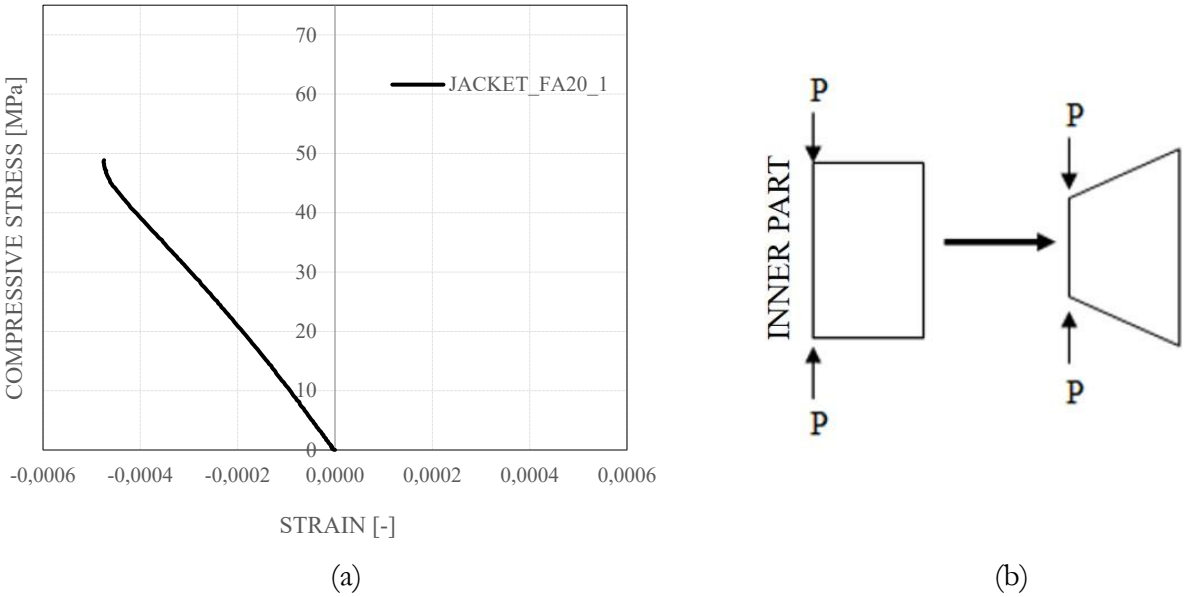

(a) (b)

Figure 2.11 - Ineffectiveness of vertical strain gauges on the jacket's surface: a) elongation; b) bending effect.

To overcome this problem, embedded strain gauges were introduced to record the vertical strain of concrete cores during the compressive test. This type of strain gauge, consisting of a 3-wires system incorporated at the center of the concrete cores, permits to obtain a more accurate value for the vertical displacement of the specimens (Figure 2.12).

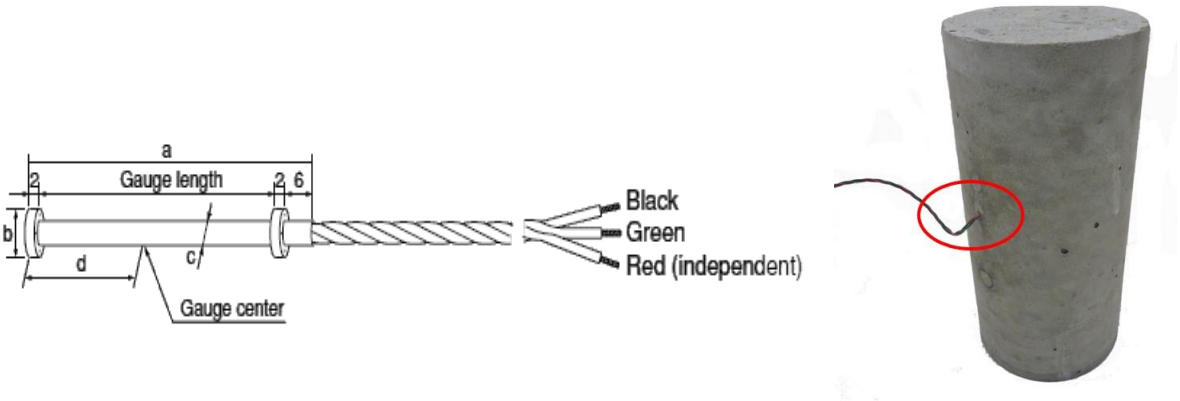

(a) (b)

Figure 2.12 - Embedded strain gauges: a) 3-wire system; b) cylindrical core with the embedded strain gauge.

During the uniaxial compression test, the deformation speed was set at 0.3 mm/min and each test was stopped when the jacket surface was completely damaged. In the following Chapter, all the results will be presented and discussed.

2.2 Mortar beams reinforced with UHP-FRCC thin layers

2.2.1 Geometrical properties

The second type of specimens analyzed consisted of prismatic mortar beams reinforced with UHP-FRCC thin layers. These reinforcement layers were designed in the bottom part of the beams in order to improve their flexural resistance.

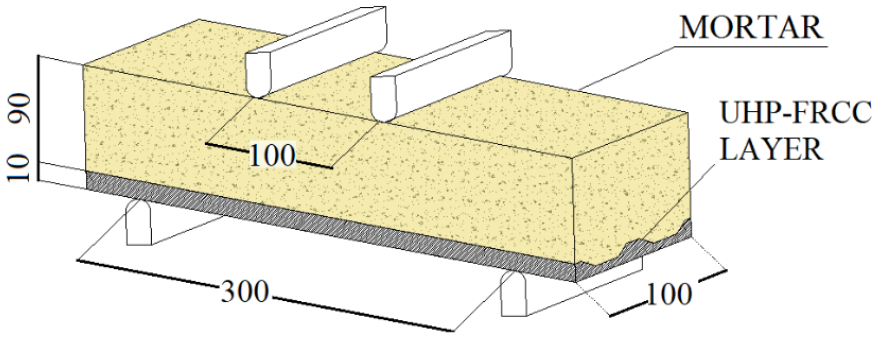

Figure 2.13 – Mortar beams reinforced with a thin bottom UHP-FRCCs layer

Considering the constant amount of UHP-FRCC used as reinforcement (10 cm^2 in the section), different solutions were proposed in order to improve the layer's efficiency.

In the first series, all the UHP-FRCC layers were realized without replacing of cement (i.e., FA0 mixture). This series was composed of 12 beams, 4 of them without reinforcement (Figure 2.14.a). In 2 beams the contact surface between mortar and UHP-FRCC was perfectly plane and smooth (Figure 2.14.b). Two more beams were designed with 30 mm steel hooked needles inserted for 20 mm in the mortar and 10 mm in the UHP-FRCC layer (Figure 2.14.c). The geometry named "A", used for other 2 beams, was composed of three trapezoidal wedges to improve the grip among the two surfaces (Figure 2.14.d). Lastly, 2 beams were designed with geometry "B" in which only one higher wedge was considered (Figure 2.14.e).

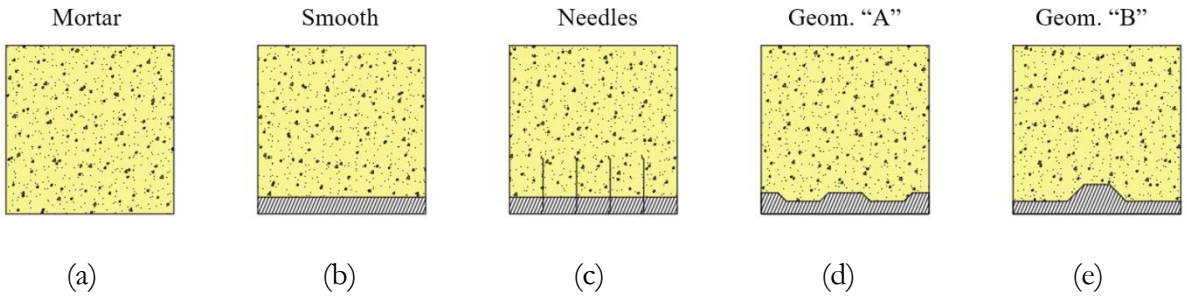

Figure 2.14 – Different boundary conditions at the contact surface (First series – FA0 mixture).

For the second series, two different UHP-FRCC mix proportions were used for 14 specimens. In 6 beams the reinforcement layer was realized with a FA20 mixture (replacement cement/fly ash ratio equal to 0.2). Other 6 beams were made with the FA70 mixture, where the 70% of total cement weight was replaced by fly ash. Finally, 2 beams were cast without reinforcement for observation. In these series, geometry "B" was omitted (Figure 2.15), because, as described in the following Chapter, the specimens reinforced with this shape were mainly influenced by delamination.

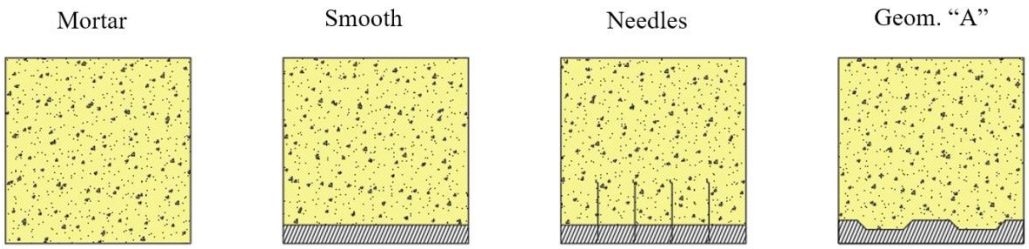

Figure 2.15 – Different boundary conditions at the contact surface (Second series – FA20 and FA70 mixtures).

Lastly, three mortar beams were reinforced not only with the UHP-FRCC bottom layers, but also placing 4 steel rebars having 20 mm of nominal diameter. For these three specimens, only reinforcement layers with geometry "A" were considered, changing the type of UHP-FRCC mixtures from FA0 to FA70.

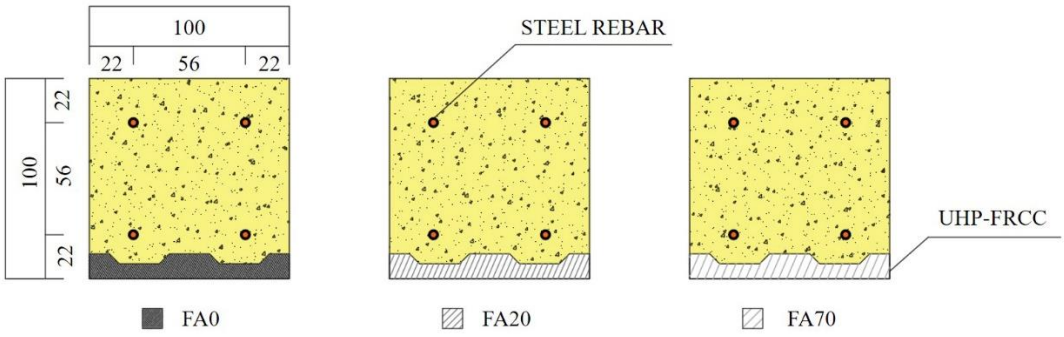

Figure 2.16 – Mortar beams reinforced with steel rebars and bottom UHP-FRCC layers.

The geometrical properties of the UHP-FRCC layers used during the experimental campaign are described in ANNEX 1. The geometrical shapes "A" and "B", designed with the Styrofoam molds, are defined in Figure 5.4 and Figure 5.5, where all the dimensions are described in mm. It is important to remark that the UHP-FRCC amount used for all the thin layers was the same, specifically 400 cm^3.

2.2.2 Material specifications

Three different UHP-FRCC mixtures were considered for the thin reinforcement layers. With respect to the absence of fly ashes (FA0 series), in FA20 and FA70 series, the replacement rates of cement with fly ash were, respectively, 20 and 70% by weight, against the overall binder content. All the mixtures were fiber-reinforced with the same steel fibers shown in Figure 2.2, using 1% of volume with micro-fibers (OL) and 1.5% of volume with macro-fibers (HDR). The Table 2.6 shows the 3 different UHP-FRCC mix proportions used to realize the thin bottom layers to improve the flexural strength of the mortar beams.

Table 2.6 – Mix proportions (wt. %) of the UHP-FRCC mixtures.

Series	Binder (B)			S / B (%)	Wo / B (%)	W / B (%)	SP / B (%)	DA / B (%)
	LH Cement / B (%)	FA / B (%)	SF / B (%)					
FA0	82	0	18	35	13	13.8	2.2	0.02
FA20	65.6	16.4						
FA70	24.6	57.4						

Note: B: binder; LH Cement: Low Heat Cement; FA: fly ash; SF: silica fume; S: aggregate; Wo: wollastonite; W: water; SP: Superplasticizer; D: defoaming agent.

The mixture ratio illustrated in Table 2.7 was considered for the mortar. High early strength Portland cement (C), sand (S) and water (W) were used, respectively, with the proportion 1:3:0.6.

Table 2.7 – Mix proportions used for mortar the mortar.

	HESP Cement (kg/m^3)	Sand (kg/m^3)	W (kg/m^3)
MORTAR	485.6	1456.9	291.4

Note: B: binder; HESP Cement: High Early Strength Cement; Sand: fine aggregate; W: water.

Cylinders with 25mm radius and 100 mm in height were tested by uniaxial compression to measure the mechanical properties of all the materials used in the experiments. The results are shown in Table 2.8.

Table 2.8 – Results of uniaxial compression on cylinders (R=25 mm, h=100 mm).

TYPE	Compressive strength (MPa)	Young's Modulus (GPa)
MORTAR (SERIES 1)	84.5	34.1
MORTAR (SERIES 2)	83.3	33.9
UHP-FRCC FA0	402.0	54.4
UHP-FRCC FA20	377.0	53.4
UHP-FRCC FA70	282.8	49.0

2.2.2 Casting and curing procedures

A significant challenge was the UHP-FRCC thin layers' implementation.

To create the specimens with needles, rectangular sponges plates (49 mm thick) were used. By including hooked needles inside these sponges, it was possible to make thin layers (10 mm thick) as illustrated in Figure 2.17.

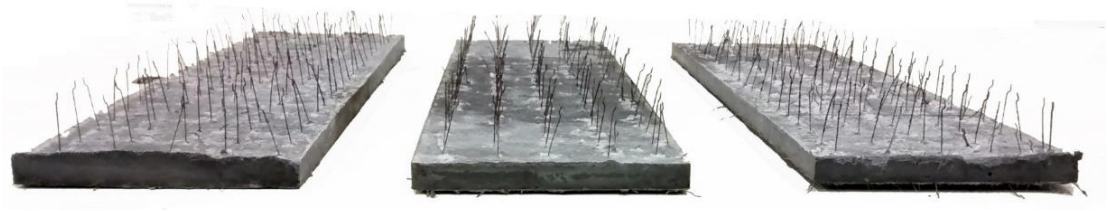

Figure 2.17 – UHP-FRCC plates with steel needles (10mm thickness).

Different Styrofoam forms were created to shape the geometry of the UHP-FRCC layers (Figure 2.18.a and Figure 2.19.a). Using a hot wire cutter, it was possible to design these forms for the reinforcement layer implementation. Geometry "A" was implemented using Styrofoam-mold with 2 trapezoidal wedges (5 mm in height). Instead, for geometry "B" was used a Styrofoam-mold with an internal trapezoidal rib (10 mm in height). Both were placed inside iron formworks with 100x100x400 mm size and covered in UHP-FRCC mixture. As results, the desired layers with different geometrical surfaces were obtained (Figure 2.18.b and Figure 2.19.b).

(a) (b)

Figure 2.18 – Geometrical layer "A": a) Styrofoam-mold used; b) the Geom. "A" reinforce layer. UHP-FRCC volume used: 400 cm^3.

(a) (b)

Figure 2.19 – Geometrical layer "B": a) Styrofoam-mold used; b) the Geom. "B" reinforce layer. UHP-FRCC volume used: 400 cm^3.

After 2 days from the UHP-FRCC cast, all the layers were subjected to steam curing for 48 hours. Later, the UHP-FRCC layers were repositioned on the bottom of different iron formworks and the mortar was cast above them (Figure 2.20). Successively, all the specimens were stored in the same humidified environment (20 °C and 95 *RH*) until the test day, performed the 21st day after the initial UHP-FRCC layers cast.

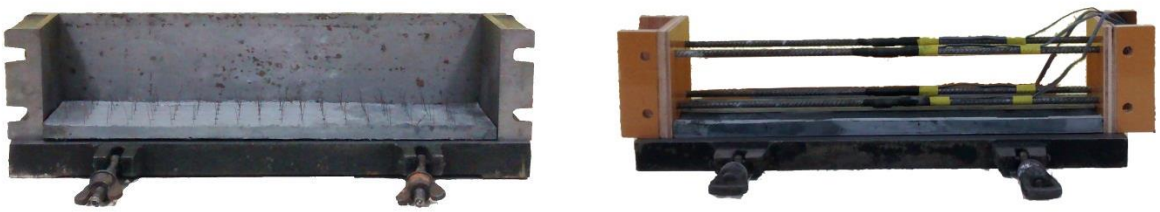

(a) (b)

Figure 2.20 – Preparation of the molds before mortar cast: a) needles plate; b) steel rebars and UHP-FRCC layer.

Both the series implemented saw the same hardening process. The whole curing procedure is illustrated in Figure 2.21, where the mortar cast moment can be identified.

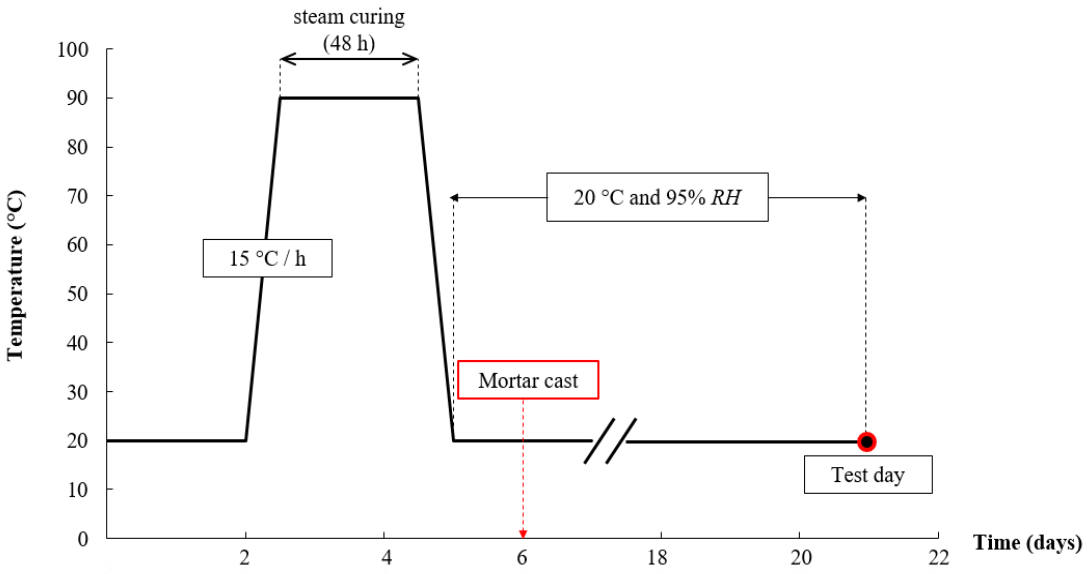

Figure 2.21 - Hardening procedure followed for all the beams.

2.2.3 Experimental devices and Test Method

For the first series, 7 strain gauges were placed on each specimen. Three of them were positioned on one lateral side, other 3 on the opposite side. A final strain gauge was placed in the middle of the UHP-FRCC bottom layer. Testing this first series, we noticed that was possible to reduce the number of strain gauges because the data recorded on the 2 opposite lateral sides were almost overlapping (Figure 2.22). For this reason, from the second series, only 4 strain gauges were placed on each beam. The strain gauges' position is shown in Figure 2.23 and Figure 2.24, depicted as the red rectangulars.

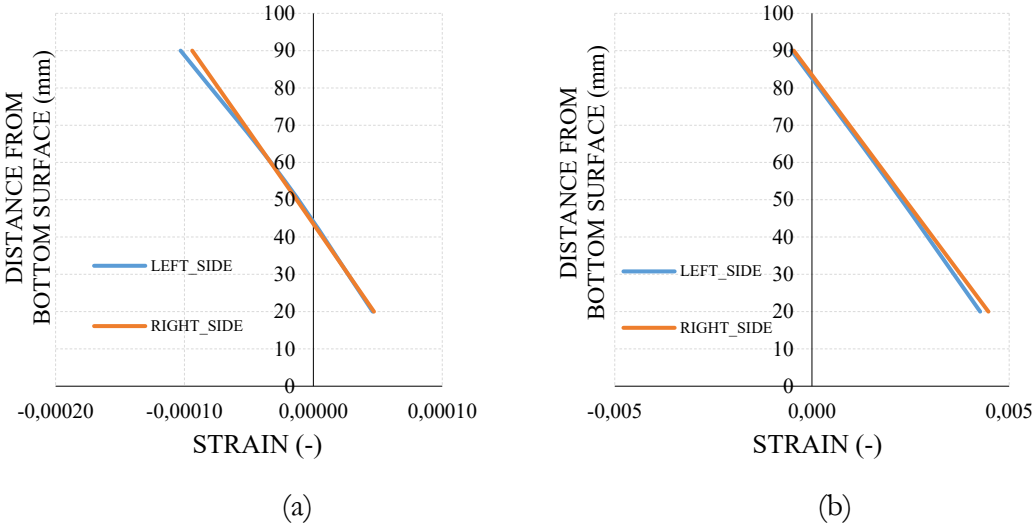

Figure 2.22 - Strain recorded by the strain gauges for different load values: a) Load max/3: b) Load max.

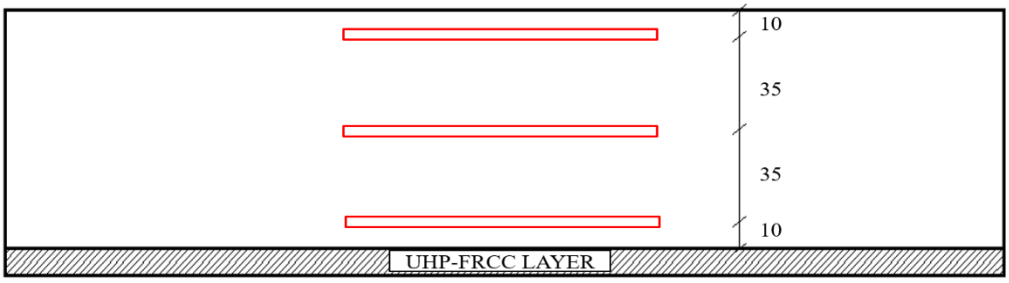

Figure 2.23 - Strain gauges' position (LATERAL SIDE).

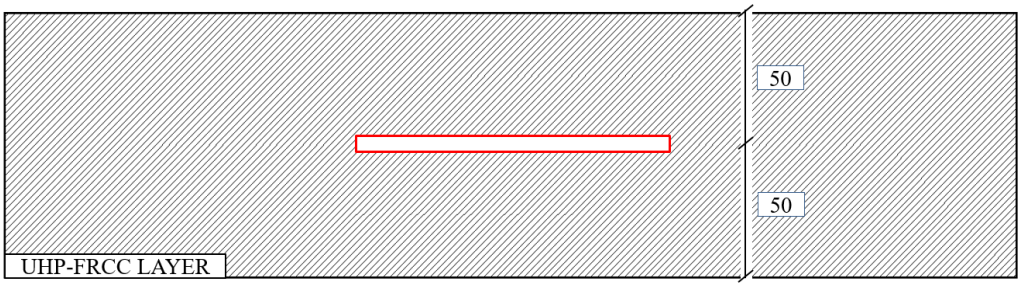

Figure 2.24 - Strain gauges' position (BOTTOM SIDE).

The specimens were tested by a four-point bending test. The loading equipment specified by JIS A 1106 - "Method of test for flexural strength of concrete" [47], is shown in Figure 2.25.a. The span length was 300 mm. The load was measured by a load cell having an accuracy within 1% of the maximum load. The flexural load was applied through consecutive load/unload cycles for pre-fixed curvature values (1/200, 1/100, 1/75, 1/50, 1/25 rad). In every cycle, the load was manually increased until the established curvature values and then gradually released.

(a) (b)

Figure 2.25 - Flexural test: a) 4-Point bending test machine; b) devices for load manual control.

The curvature measuring equipment, according to the Japan Concrete Institute Standard (JCI-S-003-2007, [48]), consist of linear variable displacement transducers (LVDTs) and jigs used for fixing LVDTs. The LVDTs, having an accuracy of 1/500 mm or higher, shall be used for measuring the axial deformation of test specimens. LVDTs, placed at positions of 15 mm and 85 mm from the lower surface of the test specimen (Figure 2.25.a), are used to measure the displacement of the pure bending span. The jigs, as shown in Figure 2.26.b, are set to allow the LVDTs rotations when it is restricted.

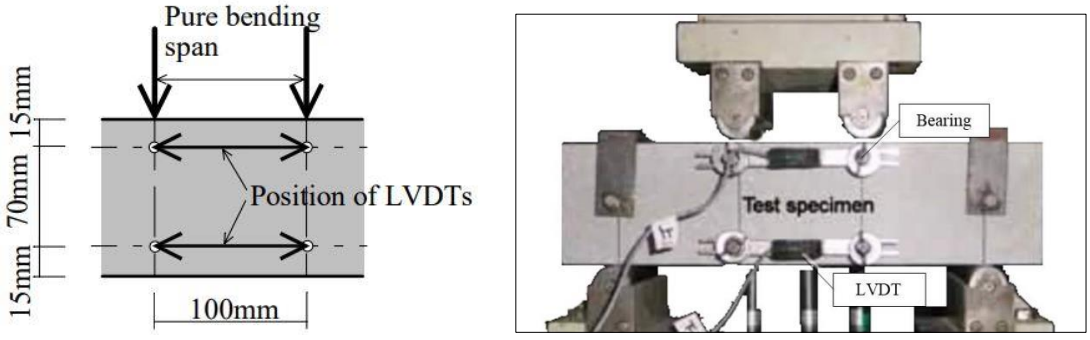

(a) (b)

Figure 2.25 - LVDTs position according to Japanese standards, pictures adapted from [48].

According to the regulations provided by the Japan Concrete Institute Standard, the bending moment was calculated using the following equation:

$$M = \frac{P}{2} \cdot \frac{l}{3}$$

where P is the applied load and l is the total span (300 mm).

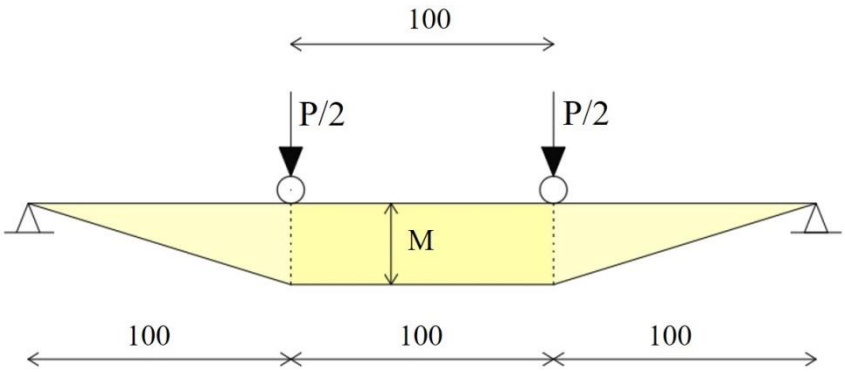

Figure 2.26 – Bending moment, 4-point bending test.

As regards the calculation of the curvature, referring to future developments the use of the data measured by the strain gauge, the values were evaluated starting from the displacement recorded directly from the machine at the middle of the beams.

In this Chapter all the aspects related to samples preparation have been illustrated. The experimental campaign included two types of specimens made of different materials. All the fresh materials properties were evaluated immediately after the cast, using the test methods presented above. The samples preparation took a long time because, after their realization, it was necessary to wait for their maturation before testing them. Two different tests were performed. Uniaxial compression test on concrete cores confined with UHP-FRCC jackets and 4-Point bending test on mortar beams reinforced in the bottom part with UHP-FRCC layers. In the following Chapter, all the results will be presented and discussed. At the beginning, the mechanical performances will be illustrated, with particular emphasis on the comparison between the three different UHP-FRCC mixtures considered. Later, the mechanical performances will be accompanied by the ecological performances provided by the UHP-FRCC manufacturing. The eco-mechanical results, obtained using the non-dimensional chart described in Chapter 1, will conclude the analysis showing a method to select the best eco-mechanical solution.

Chapter 3

Test Results and Discussion

Chapter 3

Test Results and Discussion

In this Chapter, the tests results are presented and discussed. At first, for each experiment, the mechanical results are illustrated. Then, the mechanical responses are compared with the ecological performances provided by the UHP-FRCC reinforcement. Finally, the eco-mechanical analysis is performed using the non-dimensional chart described in Chapter 1.

3.1 Concrete cylinders reinforced with UHP-FRCC jackets

The first experiment included 13 concrete cylinders cast and tested in 2 different series. In the former series, consisting of 5 cylinders, 3 of them were reinforced with UHP-FRCC jackets considering no replacing of cement with fly ash (i.e., FA0 mixture) and the other 2 were tested without reinforcement. Instead, the second series contained 8 cylinders, whose 6 were reinforced with UHP-FRCC jackets (3 with FA20 mixture and other 3 with FA70 mixture) and last 2 were left without any reinforce.

3.1.1 Mechanical performances

Uniaxial compression test were performed to estabilish the mechanical properties of concrete cylinders confined by UHP-FRCC jackets. The test were carried out under deformation control. For all the cylinders, recording forces and displacements, were obtained the stress-strain curves (from Figure 6.1 to 6.16 - Annex 2). The mechanical parameters (compressive strength, Poisson's ratio and Young's modulus) were specified in Table 6.1 and Table 6.2, set out in Annex 2.
Starting from the stress-strain curves, the average trend was calculated for each type of UHP-FRCC mixture. As illustrated in Figure 3.1, replacing part of the cement content with fly ash leads to different confinement effect on the cores and therefore different mechanical responses to the uniaxial compression (see Table 3.1). In the graph, the black continuous line is the average curve provided by the concrete cylinders confined with UHP-FRCC jackets with no fly ash substitution. The dark grey dashed line instead, represents the mechanical performance offered by the FA20 mixtures. Lastly, the grey dotted line identifies the average trend of cylinders with FA70 jackets. The comparison of all these curves with the average compressive curve of plain concrete cylinders (grey continuous line) shows that all the specimens reinforced with the UHP-FRCC jackets had a significant increase in the compressive strength.

The Young's Modulus and the Poisson's ratio were calculated, according to the Japanese standards (JIS A 1149, [49]), at one-third of the maximum load.

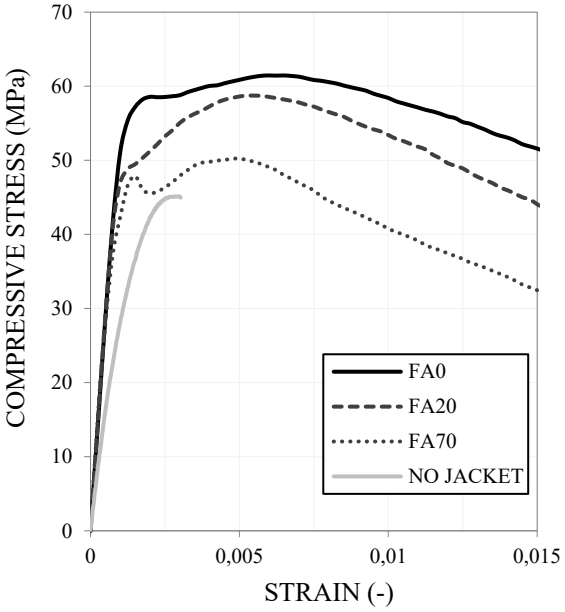

Figure 3. 1 – Compressive stress - strain relationship.

Table 3.1 – Mechanical parameters.

	Max stress [MPa]	Young's modulus Ecm [GPa]	Poisson's Ratio ν [-]
NO JACKET	45.07	34.56	0.20
FA0	61.68	37.97	0.19
FA20	59.06	37.48	0.18
FA70	50.43	35.74	0.22

In Figure 3.2, the curves are normalized dividing the compressive strength by the maximum stress reached for cores without reinforcements (fc_{core}). In case of the FA0 jackets, the resistance improvement resulted slightly less than 40%. Considering the jackets made in FA20 and FA70 mixtures, this improvement was, respectively, of 31% and 12% (Table 3.2).

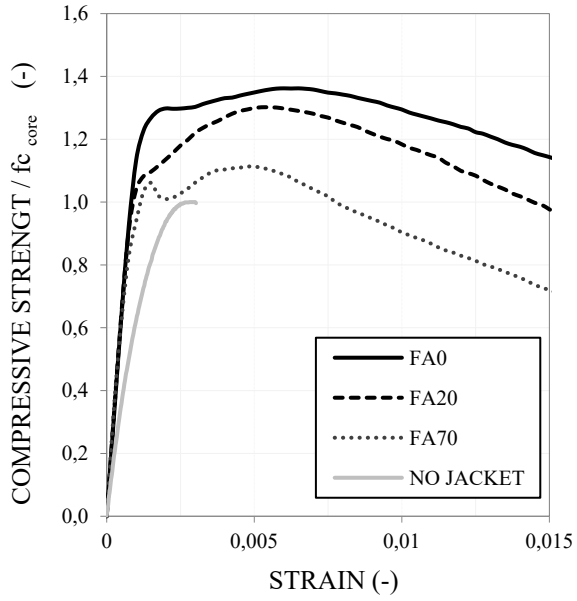

Figure 3. 2 – Compressive stress - strain relationship (Normalized with fc_{core})

Table 3.2 – Improvement due to jacketing.

	Max stress / fc_{core} (-)	Resistance increase (%)
FA0	1.37	36.85
FA20	1.31	31.05
FA70	1.12	11.89

3.1.2 Eco-mechanical analysis

Considering the results achieved through the uniaxial compression test, the mechanical performances of all the specimens were completely defined. These mechanical performances, as discussed in the previous Chapters, were compared with the ecological performances in order to select the best eco-mechanical solution. Perform this analysis without an "appropriate tool" is not so easy, because, as shown in Figure 3.3, the performances developments exhibited opposite trends. The higher the cement content in UHP-FRCC mixture used, the higher the confinement effect provided by the jacket. On the other hand, the lower the amount of fly ash used to replace the cement, the worse the ecological performances offered by the UHP-FRCC composites.

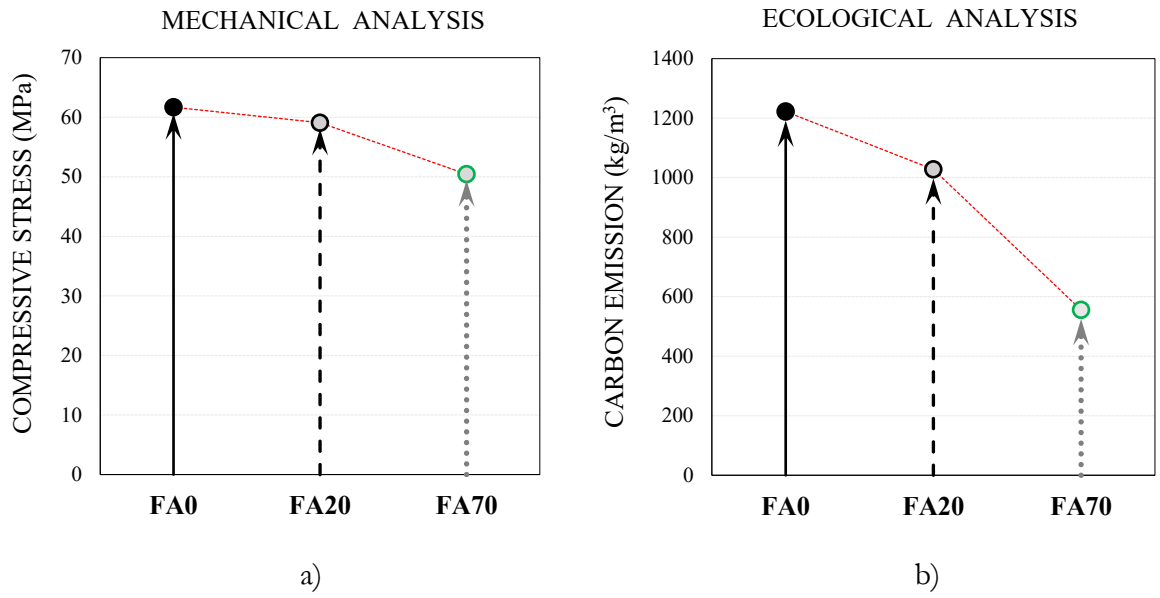

Figure 3. 3 – UHP-FRCCs mixtures' performances: a) Mechanical analysis; b) Ecological analysis.

In this study, the eco-mechanical analysis was performed using the chart described in Chapter 1. This non-dimensional diagram permits to easily view both mechanical and ecological performances, defining 4 main regions (Figure 3.4). For the concrete cores analysis, as a mechanical index (MI) was chosen the maximum compressive stress achieved during the uniaxial compression test. Furthermore, as ecological index (EI) was considered the mass of CO_2 released to produce 1 m^3 of UHP-FRCC. Both mechanical and ecological performances, assessed for all the cylinders, were related to the results achieved by the concrete cores reinforced with UHP-FRCC jackets with no fly ash substitution (FA0). Thus, the chart bounds MI_{inf} and EI_{sup} were considered, respectively, as the mechanical response and the ecological impact provided by the FA0 mixture (MI_{FA0} and EI_{FA0}).

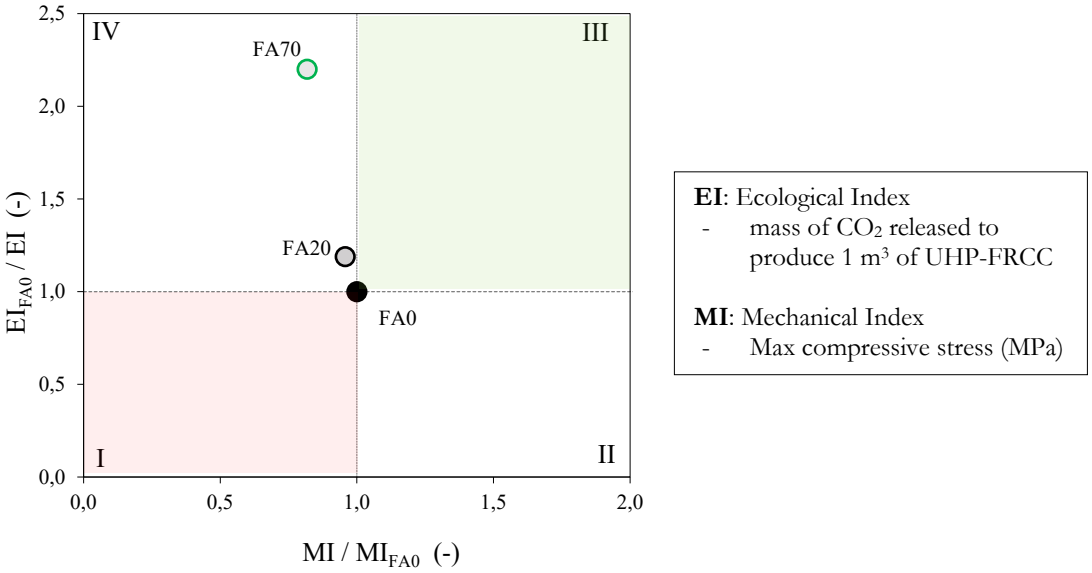

Figure 3. 4 – The eco-mechanical analysis for concrete cores reinforced with UHP-FRCC jackets.

Regarding only the mechanical performance, the best solution is to reinforce the concrete cylinders with a UHP-FRCC jacket without substitution of cement with fly ash (FA0 mixture). However, even if this solution leads to the best mechanical response, it provides also the highest ecological impact. Both the eco-mechanical results for FA20 and FA70 mixtures fall within the fourth region, in which the ecological benefits are paid in terms of mechanical performances. The compressive strength of the samples reinforced with the FA70 mixtures is significantly lower than the cores with FA0 jackets. The decrease in the confinement effect leads to a reduction of slightly less than 30% of the compressive resistance. Moreover, although the results obtained in the case of the mixture with FA20 are close to those achieved from the FA0 mixtures, they too are influenced by the decrease in the confinement effect. The replacement of 20% in weight of cement content is paid with a loss of 5% of the maximum compression strength. Anyway, jacketing the concrete cylinders provides a high improvement in the ductility of the cores, increasing the energy absorbed during the uniaxial compression.

For specimens tested under uniaxial compression, the "substitution strategy" alone seems not be sufficient to ensure high mechanical performance and low ecological impact. Indeed, the eco-mechanical analysis confirms that reducing the amount of cement used in the UHP-FRCC mixtures leads to an inevitable reduction in mechanical performances. For this reason, in the second experimental investigation, the "substitution strategy" was accompanied by the "mechanical performance strategy" described in Chapter 1.

3.2 Mortar beams reinforced with UHP-FRCC thin layer

The second experiment included mortar beams reinforced with thin bottom UHP-FRCC layers. Testing the beams under flexural loads, the underside part of the specimens resulted more severely stressed by tensile stresses. For this reason, to improve the bending resistance of these mortar beams, thin UHP-FRCC layers were designed to reinforce the samples in the bottom part, right where they were weakest.

Two series were considered: the former included only UHP-FRCC layers made of mixtures with no fly ash content (i.e., FA0 mixture), the latter also considered different fly ash amount in the UHP-FRCC mixtures (i.e., FA20 and FA70 mixtures). For the first series, different specimens were made by changing the boundary conditions between the mortar and the UHP-FRCC layer. As illustrated in the previous Chapter, some specimens were reinforced with smooth plates while other had some steel hooked needles to increase the mechanical bond. The geometry "A", was designed with 3 trapezoidal wedges (5 mm in height). Instead, for geometry "B", only 1 higher central rib (10 mm in height) were considered. Lastly, for the second series, the same typologies analyzed in the first series were implemented changing the cement content in the UHP-FRCC mixtures. It is important to notice that all the reinforcement layers had the same UHP-FRCC amount, thus variations in the mechanical response were only attributed to the boundary conditions changes or to the different cement content in the UHP-FRCC mix proportions.

3.2.1 Mechanical performances

The specimens were tested with 4-point bending test.

The flexural load was applied through load/unload cycles for fixed curvature values. For all the beams were recorded bending forces and displacements, obtaining the Moment-Curvature curves (from Figure 7.1 to Figure 7.15 - Annex 3). The maximum flexural strengths, provided by all the samples during the test, were specified in Table 7.1, set out in Annex 3.

Regarding the first series (FA0 mixture), a results comparison is illustrated in the following figures (from Figure 3.5 to Figure 3.9), where only the maximum envelopes, and not the cycles, were drawn. For each figure, the beam section, the crack at failure and the bending moment-curvature curve is depicted. With a continuous red line is represented the mechanical response to the flexural load of the selected beam. In light grey instead, are shown the other curves obtained testing the different samples during the first series experiment.

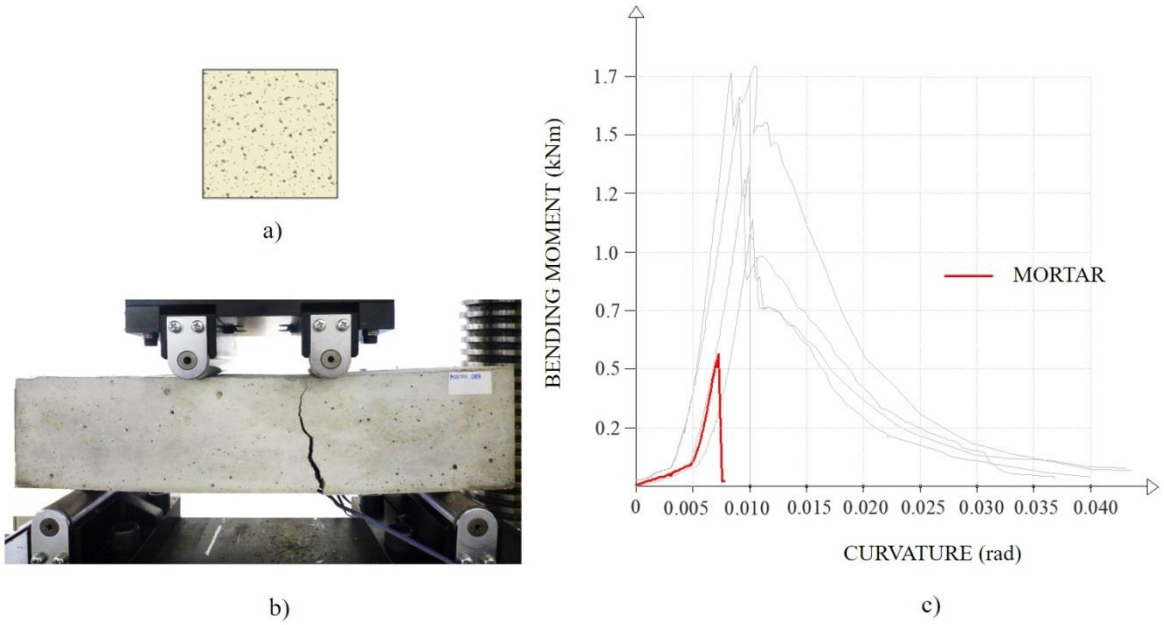

Figure 3.5 – 4-Point bending test on specimen "PLAIN MORTAR":
a) section; b) crack at failure; c) bending moment - curvature curve.

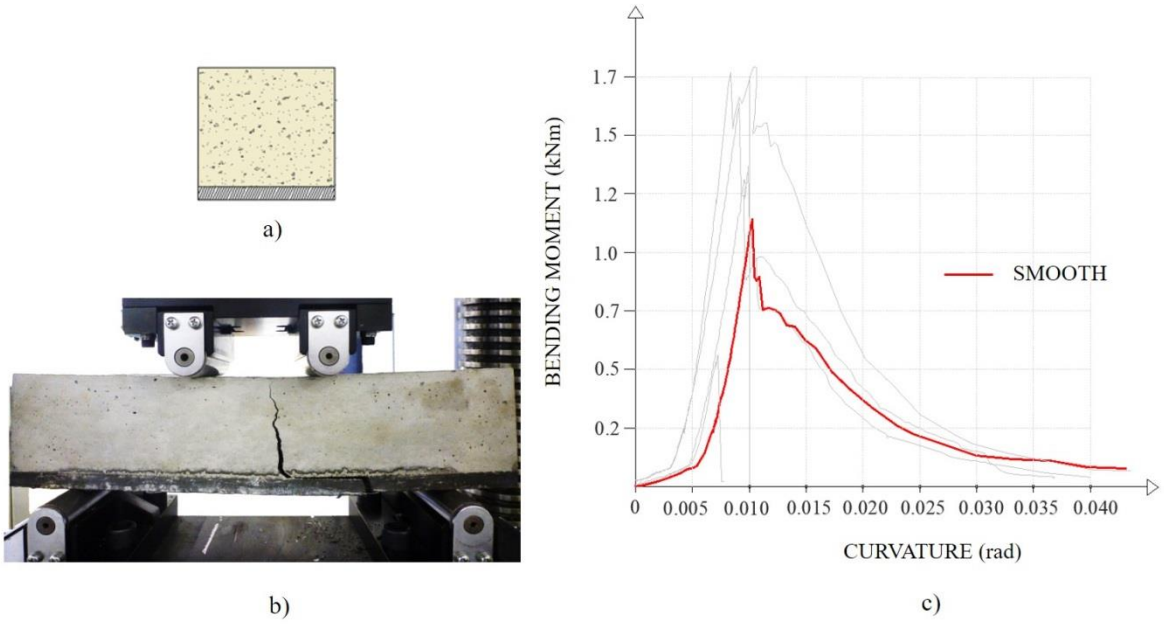

Figure 3.6 – 4-Point bending test on specimen "SMOOTH PLATE":
a) section; b) crack at failure; c) bending moment - curvature curve.

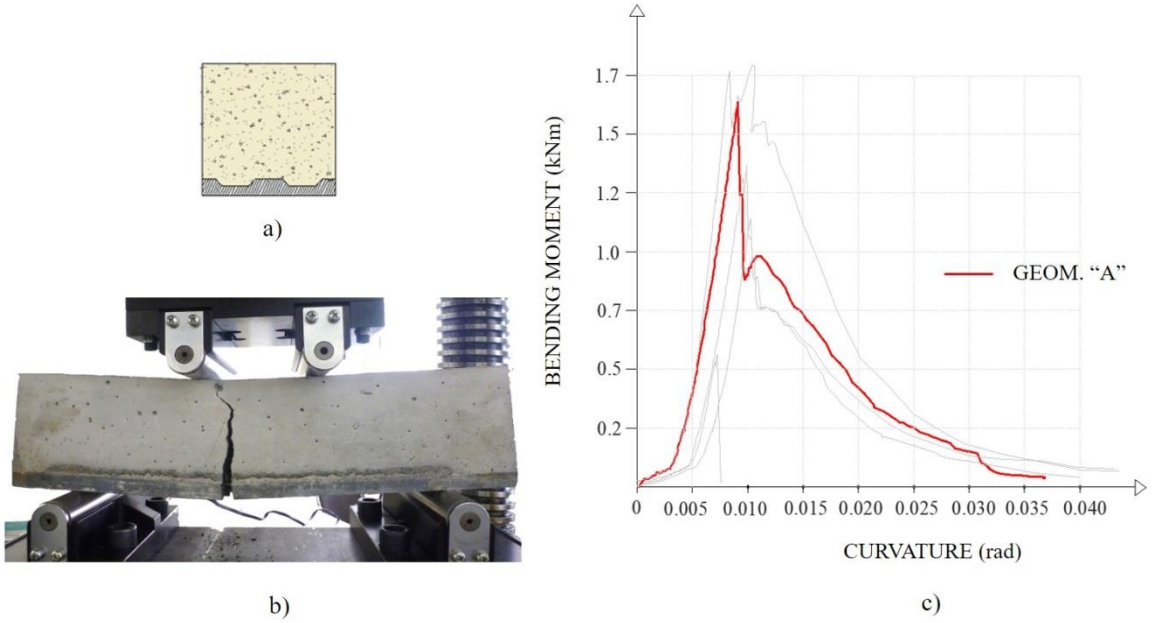

Figure 3.7 – 4-Point bending test on specimen "GEOMETRY A":
a) section; b) crack at failure; c) bending moment - curvature curve.

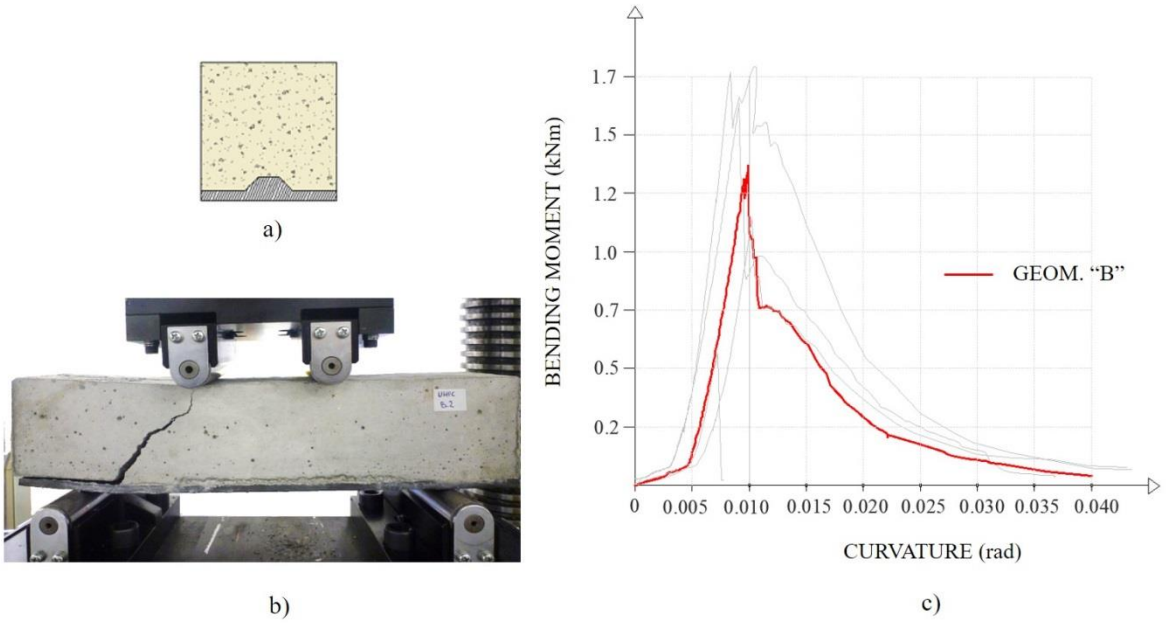

Figure 3.8 – 4-Point bending test on specimen "GEOMETRY B":
a) section; b) crack at failure; c) bending moment - curvature curve.

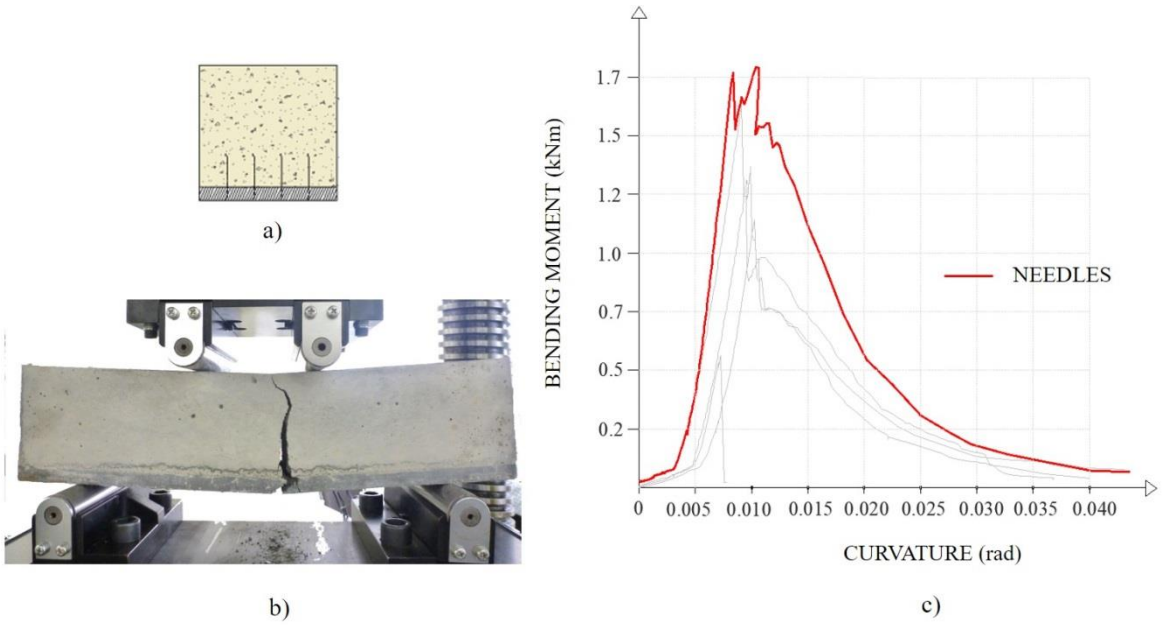

Figure 3.9 – 4-Point bending test on specimen "NEEDLES":
a) section; b) crack at failure; c) bending moment - curvature curve.

The mechanical performances, although the amount of UHP-FRCC used was the same for all the specimens, were extremely different. Indeed, where the grip between the mortar and the reinforcement layer was improved through needles or using geometrical wedges, the flexural strength was higher. As illustrated in the previous pictures, there is a connection between the crack position and the flexural strength. Proper design of the boundary condition permits to obtain beams with unified behavior between mortar and UHP-FRCC. For these specimens, the crack occurred nearly in the middle (Figure 3.7.b and Figure 3.9.b). Instead, specimens reinforced with a smooth plate or a layer with geometry "B" were more sensitive to delamination phenomena (Figure 3.6.b and Figure 3.8.b). This early detachment of the bottom layer did not allow taking full use of the UHP-FRCC's capacities, leading to lower mechanical performances.
This delamination phenomenon mainly occurs when the boundary surface is smooth. To describe this link between surface's properties and flexural resistance, a geometrical parameter named "surface complexity" *R'* was introduced as:

$$R' = \left(\frac{1}{L} \int_0^L |f(\mathrm{x})| \, \mathrm{dx} \right) \cdot \frac{L_0}{L}$$

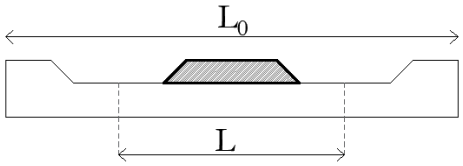

Figure 3.10 – L_0 and L definition.

where the integral represents the area of the wedge calculated within the period length L, and L_0 is the total section length (Figure 3.10).

Using this geometrical parameter *R'*, it was possible to describe the effect of the steel needles to a precise thin layer geometry (Figure 3.11).

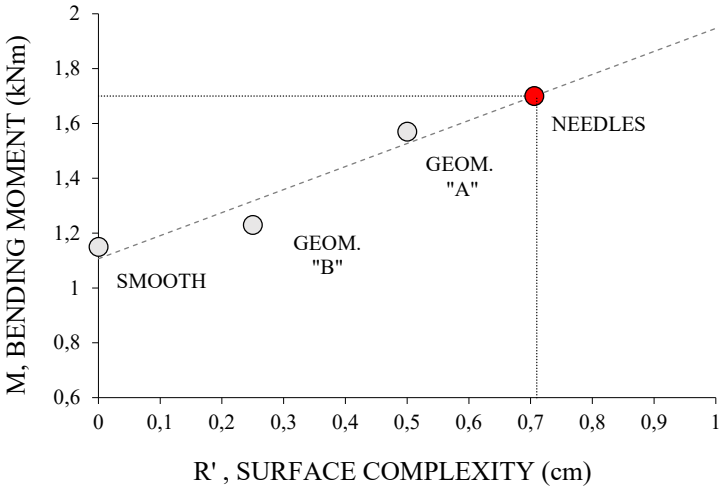

Figure 3.11 – Surface's properties and flexural resistance relationship described by *R'* (FA0 first series).

All the moment-curvature curves, obtained testing the second series, were set out in the Annex 3 (from Figure 7.7 to Figure 7.15). In this second series, reducing the cement content in the UHP-FRCC mixtures replacing part of it with fly ash, different flexural strengths were recorded (Figure 3.12). The same layers typologies studied during the first series were analyzed, except the geometry "B", who was omitted because of the delamination problem discussed above.

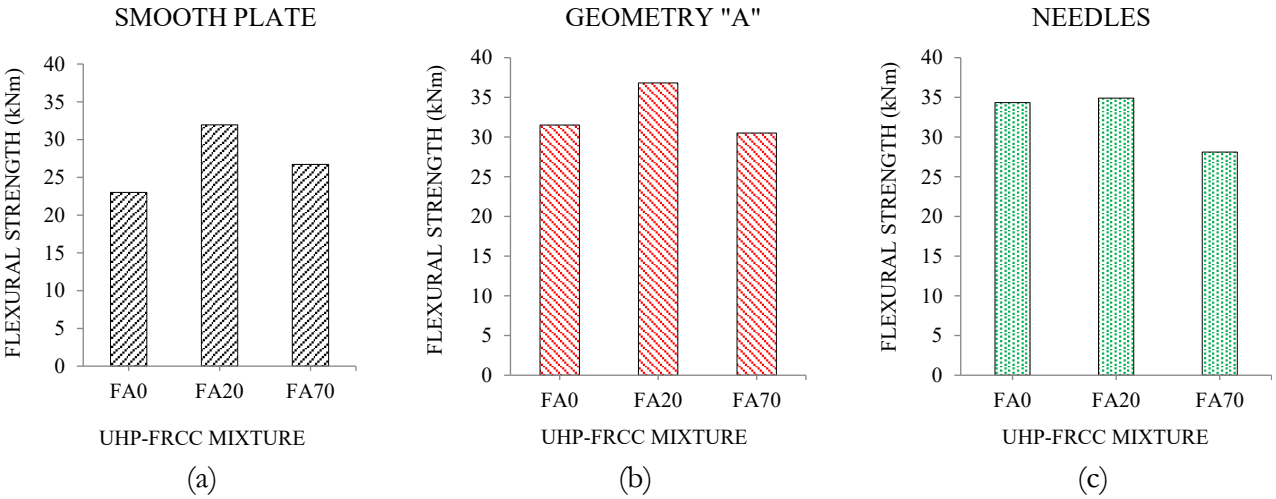

Figure 3.12 – Average flexural strength changing the UHP-FRCC mixture: a) smooth layer; b) geometry "A"; c) needles.

The mechanical characteristics, shown in detail in Table 6.1 set out in Annex 3, were used to perform the eco-mechanical analysis described in the next section. Considering the max flexural strength provided by the beams as mechanical marker, these results were compared with the ecological performances of the three different UHP-FRCC mixtures.

3.2.2 Eco-mechanical analysis

The results arising from the mechanical and ecological analysis were compared to select the best eco-mechanical solutions. As seen in the first experiment, this eco-mechanical analysis was carried out using the already mentioned non-dimensional chart.

For example, considering the specimens reinforced with geometry "A" UHP-FRCC layers, the mechanical and ecological performances show different trends (Figure 3.13).

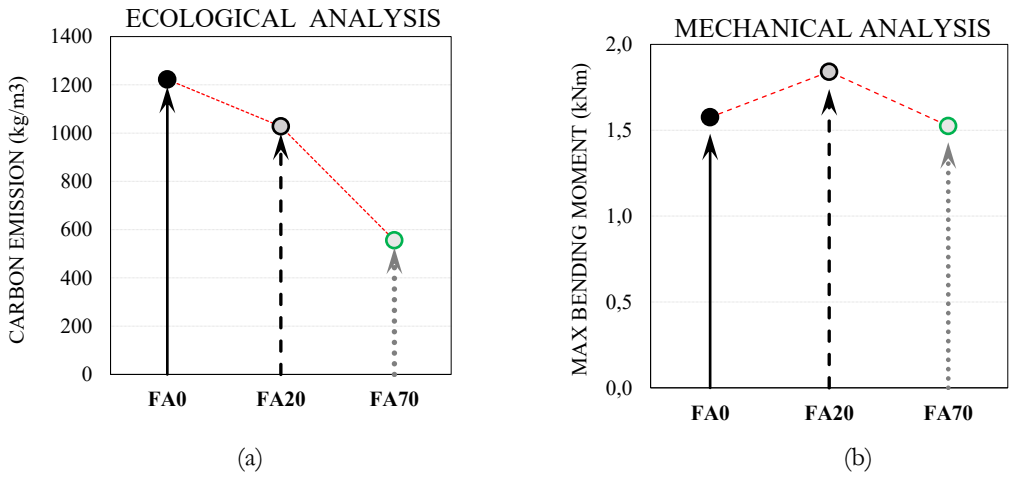

Figure 3.13 – UHP-FRCC mixtures' performances for GEOM. "A": a) mechanical analysis.; b) ecological analysis.

For the beams analysis, as a mechanical index (MI) was considered the maximum bending moment achieved during the test. Regarding the ecological index (EI), it was considered as the mass of CO_2 released to produce 1 m^3 of UHP-FRCC. Initially, the eco-mechanical analysis was referred to the FA0 mixture, assuming as chart bounds, MI_{inf} and EI_{sup}, respectively, the mechanical response and the ecological impact provided by FA0 mixture (MI_{FA0} and EI_{FA0}). The non-dimensional chart, used for the eco-mechanical analysis of "Geometry - A" performances, is shown in Figure 3.14.

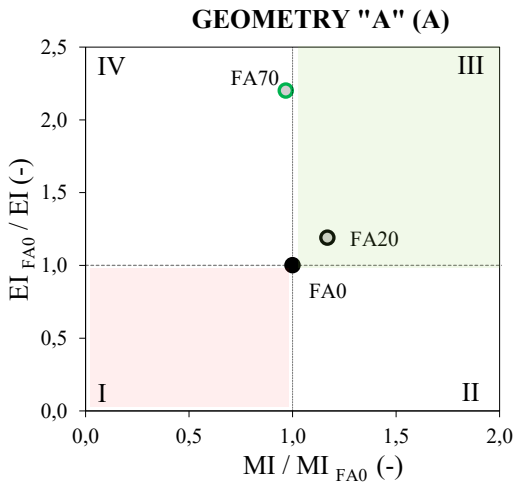

Figure 3.14 – The eco-mechanical analysis for mortar beams reinforced with UHP-FRCC thin layer (GEOMETRY "A").

According to this first analysis, the mixture with the 20% of cement amount replaced with fly ash (FA20 mixture) shown both mechanical and ecological best performances.

Performing, in the same way, this eco-mechanical analysis for all the specimens tested, the following results were obtained (Figure 3.15).

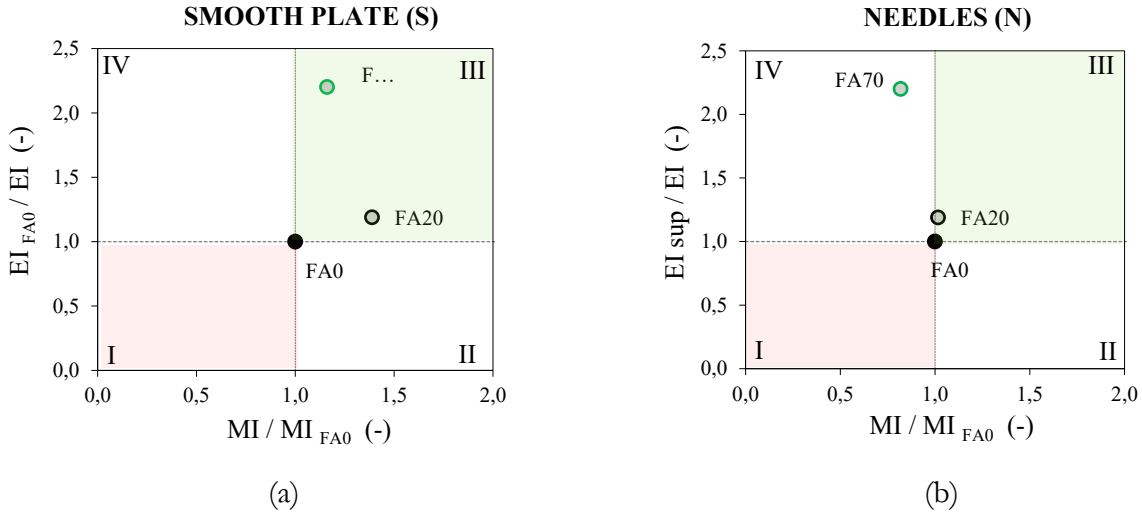

Figure 3.15 – The eco-mechanical analysis of UHP-FRCC thin layers: a) SMOOTH PLATE; b) NEEDLES.

A final comparison chart was proposed by combining all the eco-mechanical results (Figure 3.16.a). Here, to properly show the advantages offered by improving the boundary conditions of the contact surface, as a central reference point was considered the performances of mortar beams reinforced with a smooth plate in UHP-FRCC with FA0 mixture (0-S).

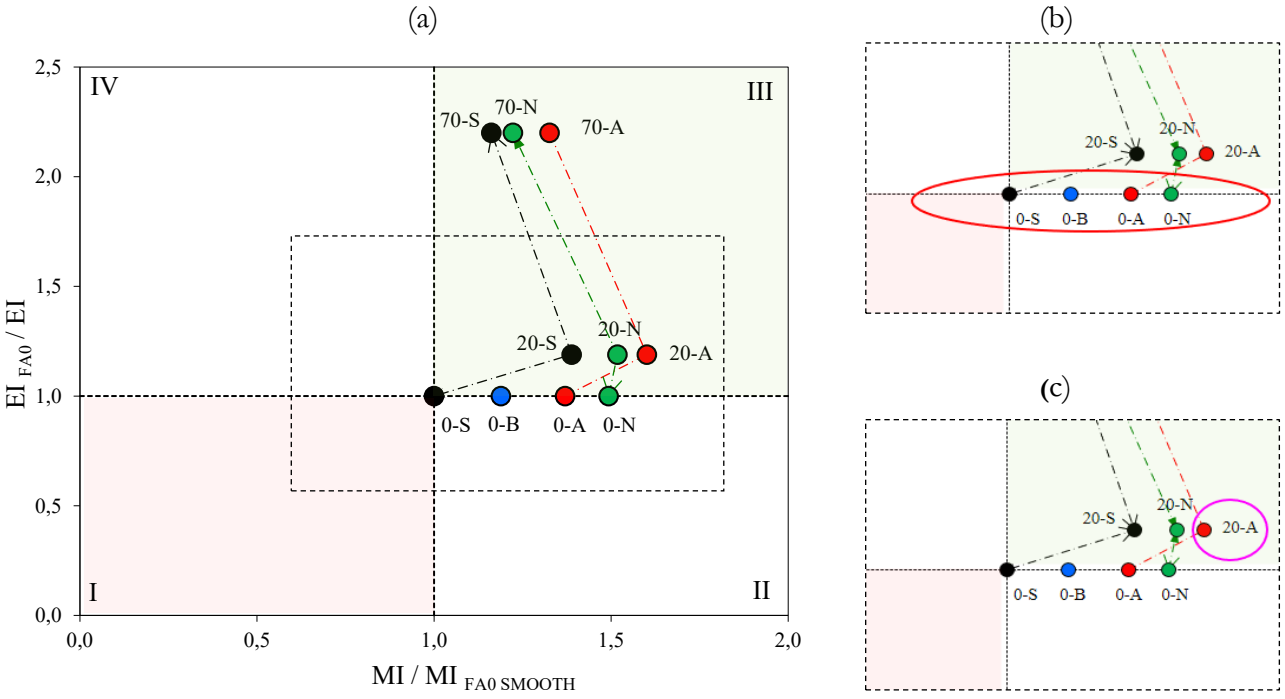

Figure 3.16 – Eco-mechanical analysis (Final comparison chart).

According to the "mechanical performance strategy", or better, not considering any substitution of cement with fly ash (only FA0 mixture), the best solution is provided by the UHP-FRCC thin plates with steel needles (Figure 3.16.b). Furthermore, considering both "substitution" and "mechanical performance" strategies, the best solution is identified by the 20-A point (Figure 3.16.c). Thus, taking into account both the ecological strategies described, the best way to reinforce a mortar beam with a thin layer in UHP-FRCC is to shape the contact surface with the geometry "A" and to replace the 20% of cement mass with fly ash. Also, the eco-mechanical results of mortar beams reinforced with steel bars and UHP-FRCC bottom layer designed with geometry "A" seems to support that this choice allows to reach the best eco-mechanical solution. Indeed, also in this situation, referring the non-dimensional chart to the FA0 performances, the point describing the FA20 mixture falls within the third region (Figure 3.17). The replace of 70% of cement mass with fly ash still leads to a significantly decrease in the flexural resistance of the beam. The high reduction of the ecological impact is paid in term of mechanical response to the flexural stress, and the point FA70 is located in the fourth zone.

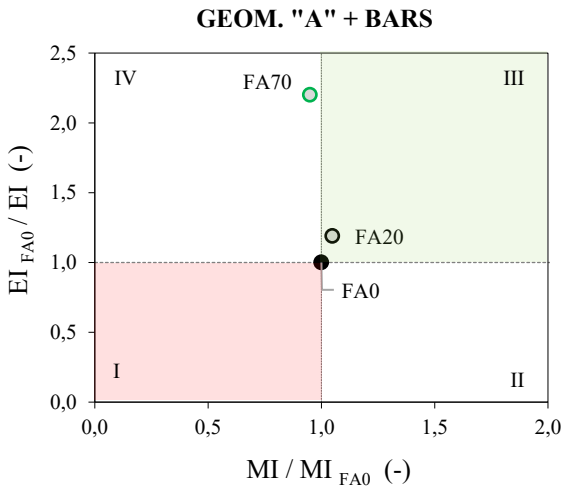

Figure 3.17 – The eco-mechanical analysis for beams reinforced with steel bars and UHP-FRCC layers with Geom. "A".

In this second experimental investigation, unlike the concrete cores samples, supporting the "substitution strategy" with the "mechanical performance strategy" allowed to propose solutions with lower ecological impact and higher mechanical performances. The geometry "A", with its trapezoidal wedges, improved the mechanical bond between the mortar and the reinforcement layer. In this way, the final reinforced beams took full advantage of UHP-FRCC's presence and showed higher flexural resistance. Moreover, in case of bending loads, the partial substitution of a small part of cement with fly ash did not seem to have decreased the mechanical response, instead, it provided a better mechanical behavior.

In this Chapter all the experimental results obtained during the test were discussed. Both the experimental investigations shown the mechanical benefits achieved using the UHP-FRCC composites to reinforce concrete cylinders and mortar beams. In the first experience, placing UHP-FRCC jackets around the concrete cores enhanced their mechanical response under uniaxial compression test. Aiming to reduce the high ecological impact of the UHP-FRCC mixtures, caused to the large amount of cement present in these cementitious composites, part of the cement mass was replaced with fly ash, in order to select a eco-friendlier material. The results of the compression test on the cores showed that lowering the amount of cement in favor of fly ash decreases also the mechanical performances of the cores, reducing the effect provided by the jackets. The eco-mechanical analysis was performed with the non-dimensional chart described in Chapter 1, which permits to easily compare together ecological and mechanical performances. This analysis illustrated the inefficacy of the "substitution strategy" for concrete cylinders under compression tests, when it is applied alone.

In the second experience, mortar beams were reinforced putting thin UHP-FRCC layers in their bottom part. Different samples were implemented changing the condition at the contact surface between the mortar and the reinforcement layer. Also, three distinct UHP-FRCC mixtures were prepared varying the cement content in the mix. The mechanical results, obtained testing the beams under flexural loads, showed that changing the surface properties of the reinforcement layers allows to achieve different flexural strength. Still using the eco-mechanical chart, it was possible to select the best eco-mechanical solutions among the different combinations proposed. The final comparison showed that, if the mechanical bond between the mortar and the UHP-FRCC layer is improved through a proper design, it is possible to reduce the amount of cement without compromising the mechanical performances but also increasing the flexural resistance. Indeed, the light substitution of the 20% of cement content with fly ash permits to increase both the ecological and mechanical performance provided by the UHP-FRCC bottom layers.

Finally, in the next Chapter, all these results will be reclaimed to draw the conclusions of the study, and some possible future development will be suggested.

Chapter 4

Conclusions and Future Research

Chapter 4

Conclusions and Future Research

Use of ultra-high performance fiber reinforced cementitious composite (UHP-FRCC) allows improving the mechanical performances of specimens made of concrete and mortar. In this work, two experimental investigations were carried out:

1. plain concrete cylinders confined with UHP-FRCC jackets;
2. mortar beams reinforced with thin UHP-FRCC layers.

Cylindrical concrete cores were reinforced using UHP-FRCC jackets. These jackets, providing a lateral confinement effect on the cores, enhanced the compressive strength, ductility and stiffness of the concrete cylinders tested by uniaxial compression tests. Mortar beams, subjected to flexural loads, were also strengthened by placing thin UHP-FRCC layers in their bottom part. Indeed, reinforcing a selected zone of the beams with UHP-FRCC allowed increasing the specimens' bending resistance. However, although the UHP-FRCC's use improves the mechanical responses, it causes a high ecological impact due to the copious amount of cement used in the UHP-FRCC's mixtures. The cement production is responsible for large CO_2 quantities released into the environment, due mainly to the calcination of limestone and the high energy consummate during manufacturing. To decrease the ecological impact, two main strategies were developed in this study.

The "substitution strategy" consists of replacing part of cement amount with fly ash, a waste by-product derived from coal burning. As described in [20] and [21], it releases low quantities of CO_2. Thus, replacing part of the cement content with fly ash could be an effective way to improve also the ecological properties of UHP-FRCC composites. Three UHP-FRCC mixtures were prepared considering different cement amounts. With respect to the absence of fly ashes (FA0 series), in FA20 and FA70 series, the replacement rates of cement with fly ash were, respectively, 20% and 70% by weight, against the overall binder content.

The "mechanical performance strategy" suggests to improve the design of the UHP-FRCC reinforcement layers aiming at enhancing the mechanical performance of the beams under flexural loads. Indeed, ensuring good properties of the mechanical bond between the mortar and the UHP-FRCC layer, higher flexural strengths can be obtained. Thus, it is possible to reduce the amount of UHP-FRCC required to achieve the same mechanical resistance.

Both these strategies were implemented to select the best eco-mechanical solution among different proposed combinations. The eco-mechanical analysis was performed using the non-dimensional chart proposed by Fantilli and Chiaia [1]. This non-dimensional graph allows to compare together both ecological and mechanical performances through the Mechanical Index (MI) and the Ecological Index (EI). The former identifies the mechanical performance of the samples and it can be described with different mechanical parameters depending on the test performed, such as the maximum compressive stress, the maximum flexural load or the energy absorbed. The latter regards the ecological aspect related to the UHP-FRCC manufacturing. In this work, it was considered as the mass of CO_2 released by the production of 1 m^3 of UHP-FRCC.

In the first experimental campaign, the compression tests on the cylindrical cores confirmed that the confinement effect provided by the jackets enhanced the compressive resistance of the concrete cylinders. Such improvement was related to the mix proportion used for the UHP-FRCC jackets. The higher the cement content in the mixture, the higher the confinement effect on the cores. The compressive strength of cylinders reinforced with jacket made with FA70 mixture was significantly lower than the cores with FA0 jackets. The reduction of the confinement effect caused a loss of 30% in compressive resistance. Moreover, even though the results provided by the FA20 jackets were close to those achieved from the FA0 mixtures, they too were affected to the confinement effect decrease. The replacement of 20% in weight of cement content was paid with a loss of 5% of the maximum compression strength. Nevertheless, all the cylinders confined by these UHP-FRCC jackets showed a significant improvement in the ductility, increasing the energy absorbed during the uniaxial compression test.

The application of the "substitution strategy" alone permitted to reduce the environmental impact but also reduced the confinement effect. The ecological benefits were paid in term of mechanical resistance. To overcome this problem, in the second experiment, this ecological strategy was joined with the "mechanical performance strategy". Mortar beams were reinforced with thin UHP-FRCC layers in order to increase the flexural strength provided in 4-point bending test. Different samples were implemented changing the design of the UHP-FRCC reinforcement layer. Some beams were reinforced using steel needles arranged between mortar and UHP-FRCC layer. This solution enhanced the grip of the layer and ensured a unified behavior among the two different materials. The mechanical response of these beams resulted higher compared with the mechanical performance provided by the same specimens without needles. Also, two separate surface shapes were designed considering constant the amount of UHP-FRCC used to reinforce. The geometry "A" had three trapezoidal wedges used to better

interlock the layer to the plain mortar. Instead, for geometry "B", only one higher rib were placed in the central part of the UHP-FRCC surface. The test results revealed that geometry "A" is more suitable to reinforce the beams because the samples reinforced with this shape resulted less affected to the layer delamination. Indeed, the precence of three wedges on the UHP-FRCC surface ensured good mechanical bond with the upper mortar. On the other hand, in geometry "B" the higher number of smooth part made the layer more weak and sensitive to detachment. To describe this connection between shape properties and flexural response a geometric parameter was introduced. This parameter, called "surface complexity" *R'*, allowed to relate the effect of the steel needles to a precise thin layer geometry. As done for the concrete cores jackets, also in this second experience the three different UHP-FRC mixtures, above described, were prepared and their performances compared. Performing the eco-mechanical analysis, it was possible to select the best solution among those previously proposed. According only to the "mechanical performance strategy", or better, not considering any substitution of cement with fly ash (FA0 mixture), the best way to reinforce the beams is to consider a thin bottom UHP-FRCC layer with steel needles. This solution provided the best mechanical performances leaving unchanged the ecological impact. However, considering both "substitution" and "mechanical performance" strategies, it was possible to reach results with higher flexural strength and lower environmental costs. Indeed, the eco-mechanical analysis showed that replacing the 20% of cement mass with fly ash (FA20 mixture) and designing the layer surface with geometry "A" represents the best eco-mechanical solution. In this way, the reinforced beams took full advantage of UHP-FRCC's presence and provided the higher flexural resistance. Moreover, in case of bending loads, the partial substitution of a small part of cement with fly ash did not show any decrease in mechanical response, instead, it provided a better mechanical behavior. These considerations were also confirmed by the experimental observations obtained testing the beams reinforced, not only with UHP-FRCC layers, but also by placing steel bars inside the specimens (4 steel rebars having 20 mm of nominal diameter). Here again, the replacement of 70% of the cement content (FA70 mixture) has been paid with the substantial losses of the mechanical resistance. On the other hand, a substitution of 20% of cement mass with fly ash (FA20 mixture) did not affect the mechanical response of the beams, but also it provided the highest flexural strength. In conclusion, this second experimental campaign proposed the combined use of the layer with three wedges (geometry "A") with the mixture made of 20% of cement replace, to increase the mechanical performances and to reduce the ecological impact of the UHP-FRCC reinforcement.

Based on the results of the experimental investigation previously described, the following conclusions are drawn:

- The confinement effect provided by the UHP-FRCC jackets on plain concrete cylinders increases the compressive strength, Young's modulus and ductility under uniaxial compressive test;

- Although the replacing part of cement with fly ash reduces the confinement effect provided by the jacket, this substitution drastically decreases the ecological impact of UHP-FRCC composites ("material substitution strategy");

- Placing thin UHP-FRCC layers in the bottom part of mortar beams enhances the flexural strength, the bearing capacity and the ductility under 4-point bending test;

- The analysis of the boundary conditions should be considered as a significant parameter during the beams reinforcement. A proper geometrical shape of the bottom layer allows to achieve higher mechanical performance reducing the UHP-FRCC required ("mechanical performance strategy");

- Using the non-dimensional eco-mechanical chart proposed in [1], it is possible to easily assess both mechanical and ecological performances simultaneously with the aim to select the best solution among the different proposed options;

- The combined use of both the design strategies described, makes it possible to reduce the ecological impact of the UHP-FRCC reinforcement, without compromising the mechanical benefits, but it also allows to reach higher strength performances.

Possible future developments can be suggested to complete what is proposed in the present work. This study was mainly inspired by the period of study spent at the Tohoku University of Sendai (Japan). There, I was able to use the laboratories of the host university to create and test the specimens shown in this study. In the future, an analytical model describing the behavior of concrete confined with the UHP-FRCC jackets should be presented. According to the studies illustrated in [29,30,31,32], a theoretical stress-strain model for confined concrete can be proposed. The experimental investigation described in this Thesis could be used to validate this analytical model. Through the model will be possible to perform virtual tests by changing the jacket thickness and the UHP-FRCC mixtures. In this way, new eco-mechanical analysis could be arranged still referring to the non-dimensional chart proposed in [1]. Regarding the second experiments, new tests should be performed varying the shapes of the reinforcement layers. Also, an analytical model should be proposed to describe the connection between the delamination and the geometrical properties of the UHP-FRCC surfaces. In this work, the "surface complexity" parameter (*R'*, see Chapter 3) was referred only to the performances provided by the samples reinforced with FA0 mixture. Hence, to improve the design of new UHP-FRCC layers, new tests should be performed to better set the geometrical parameter proposed. Furthermore, in this analysis, according to the "material substitution strategy", three different UHP-FRCC mixtures were prepared. The study showed that high substitution of cement mass with fly ash decreases the mechanical properties of UHP-FRCC composites. Despite the mixture with the 70% of cement content replaced by fly ash (FA70) drastically reduced the ecological impact of UHP-FRCC reinforcement, this mixture provided also the worst mechanical characteristics. However, when the replacement cement rate was about the 20%, not only the ecological, but also the mechanical performances of the UHP-FRCC were enhanced. For this reason, in the future, new UHP-FRCC mixtures should be prepared by focusing on intervals around 20%, instead of higher replacement rates.

Annexes

Annex 1

Geometrical properties

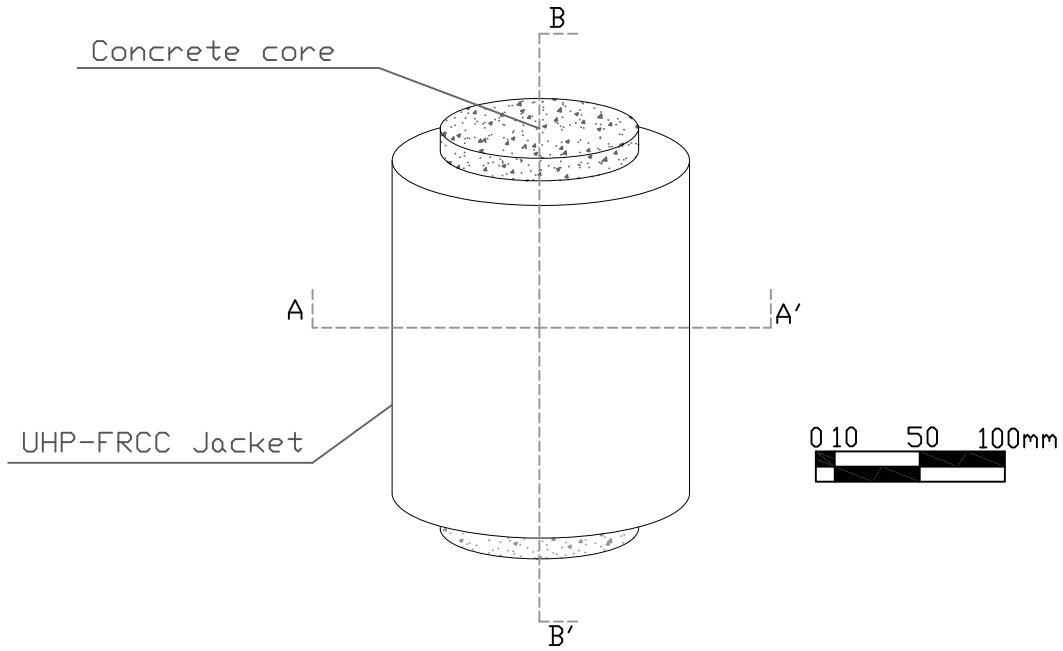

Figure 5.1 - Concrete cylinders reinforced with UHP-FRCC jackets.

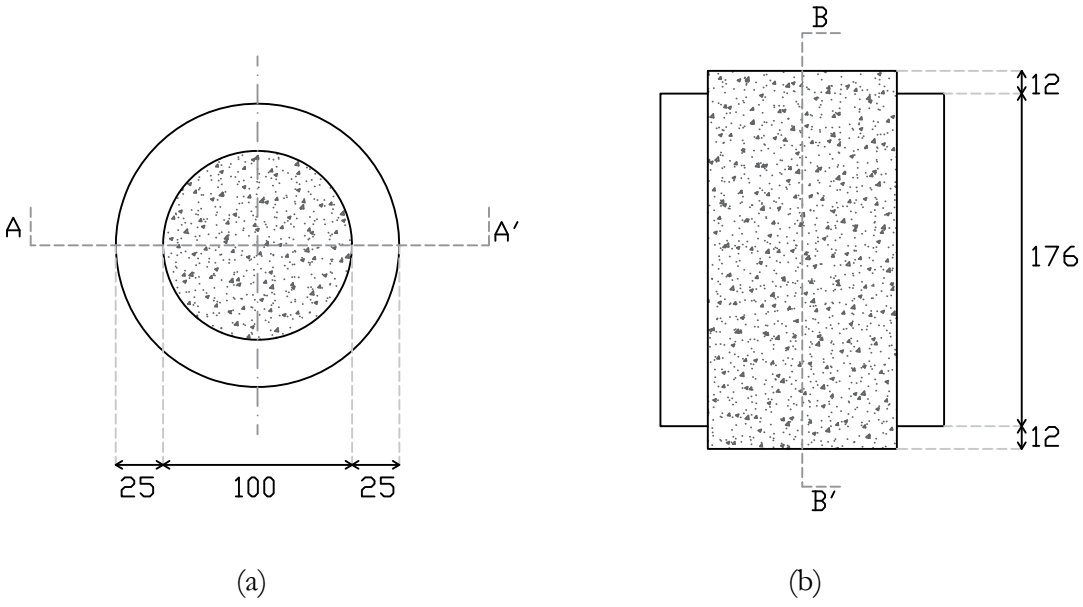

Figure 5.2 - Sectional views: a) Sez. A-A'; b) Sez. B-B'.

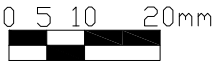

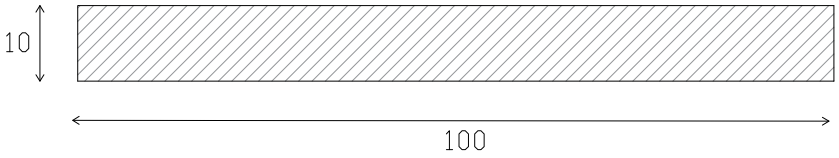

Figure 5.3 - UHP-FRCC layer type: smooth plate.

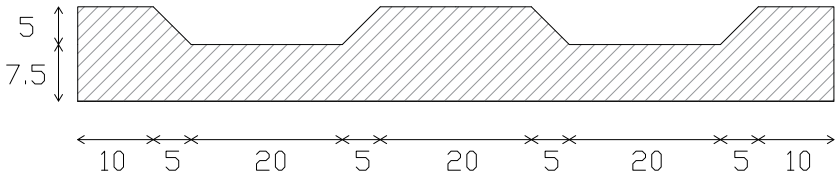

Figure 5.4 - UHP-FRCC layer type: geometry "A".

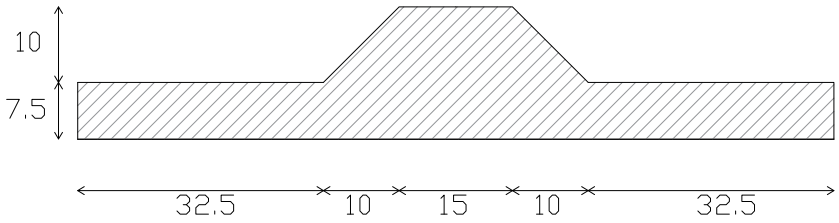

Figure 5.5 - UHP-FRCC layer type: geometry "B".

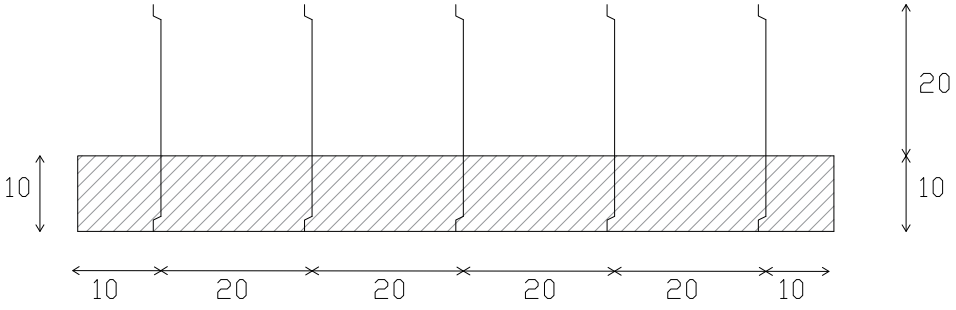

Figure 5.6 - UHP-FRCC layer type: plate with needles.

Annex 2

Uniaxial Compression Test

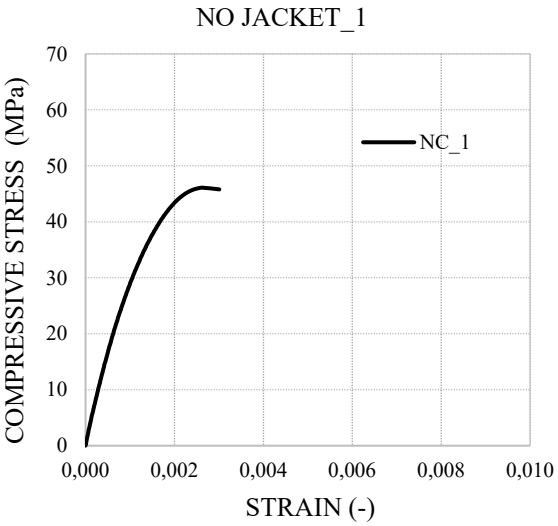

Figure 6.1 – Stress - strain curves: concrete cylinder 1.

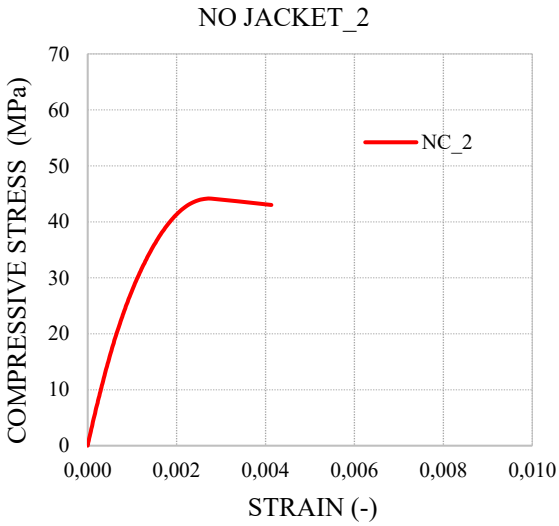

Figure 6.2 – Stress - strain curves: concrete cylinder 2.

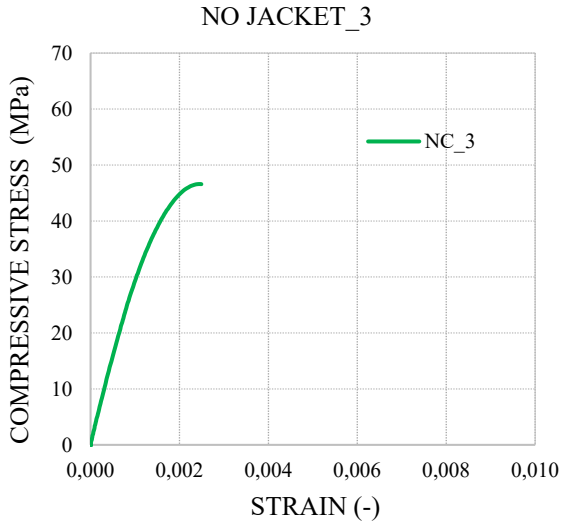

Figure 6.3 – Stress - strain curves: concrete cylinder 3.

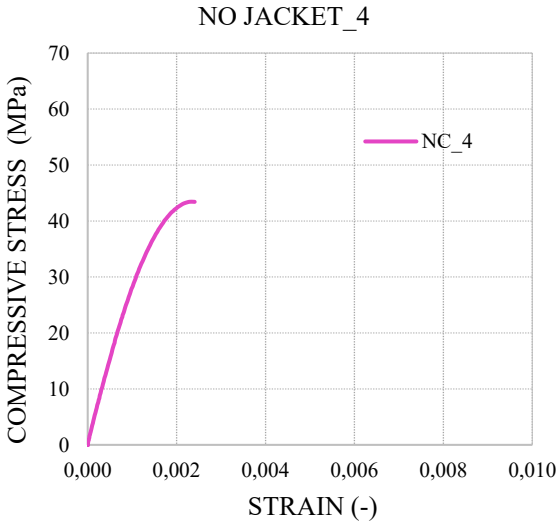

Figure 6.4 – Stress - strain curves: concrete cylinder 4.

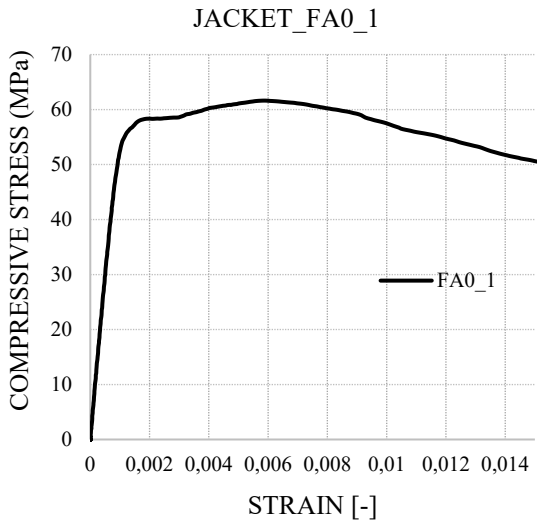

Figure 6.5 – Stress-strain curves: jacket FA0_1.

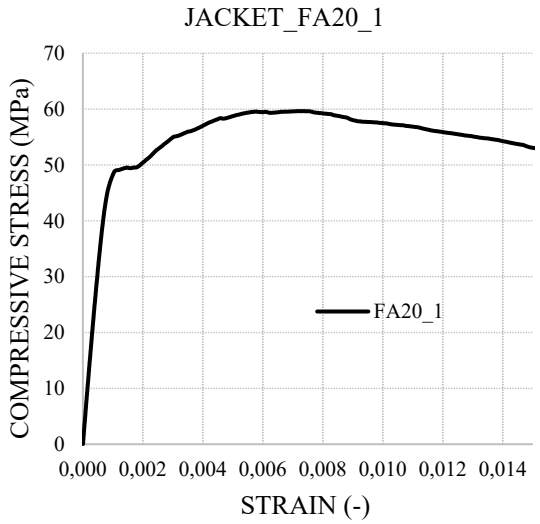

Figure 6.6 – Stress-strain curves: jacket FA20_1.

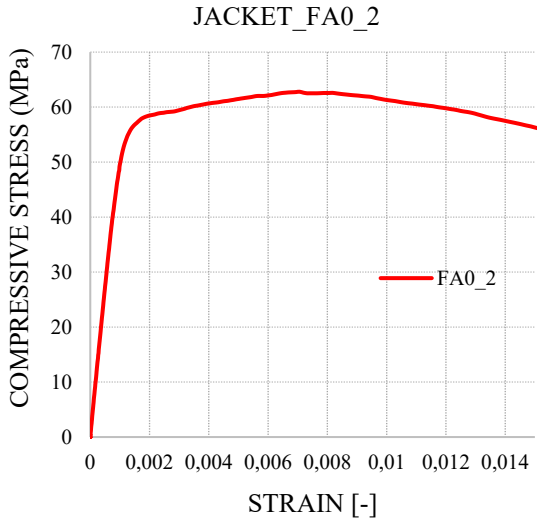

Figure 6.7 – Stress-strain curves: jacket FA0_2.

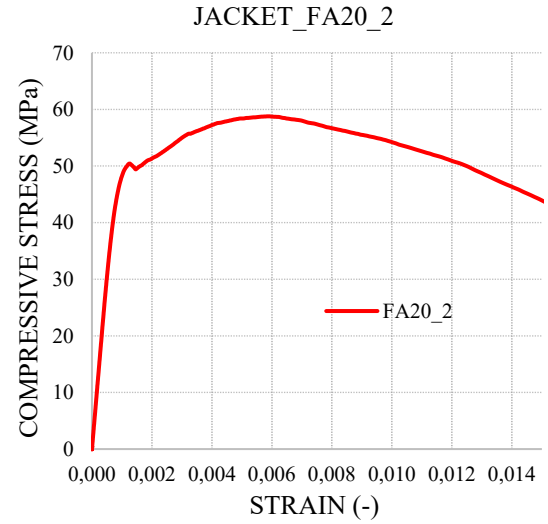

Figure 6.8 – Stress-strain curves: jacket FA20_2.

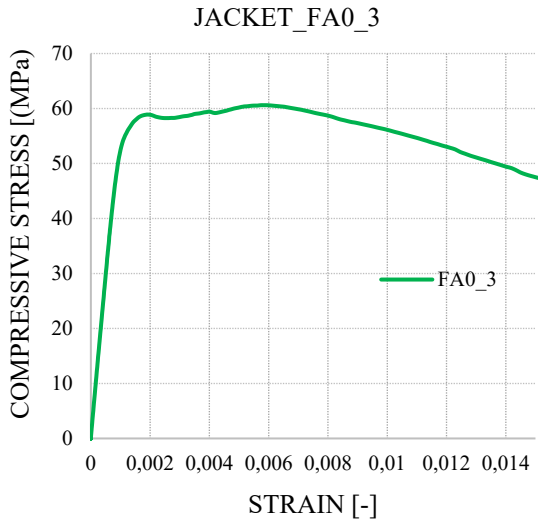

Figure 6.9 – Stress-strain curves: jacket FA0_3.

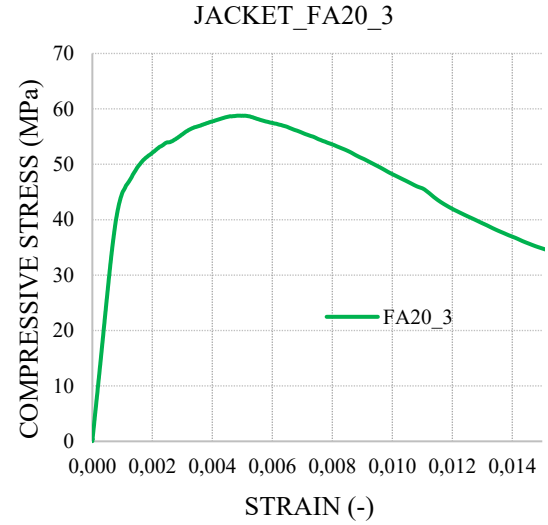

Figure 6.10 – Stress-strain curves: jacket FA20_3.

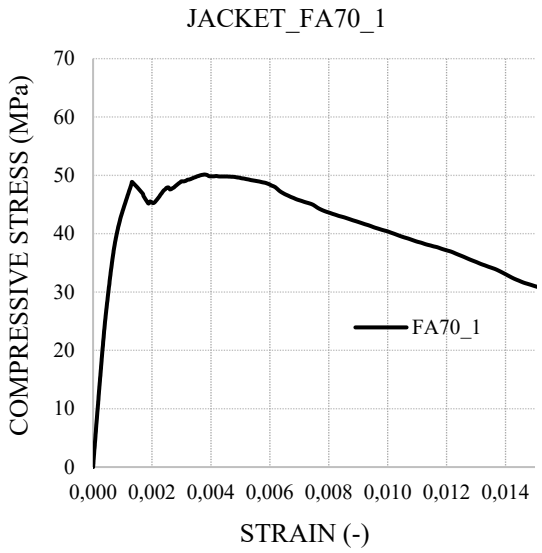

Figure 6.11 – Stress-strain curves: jacket FA70_1.

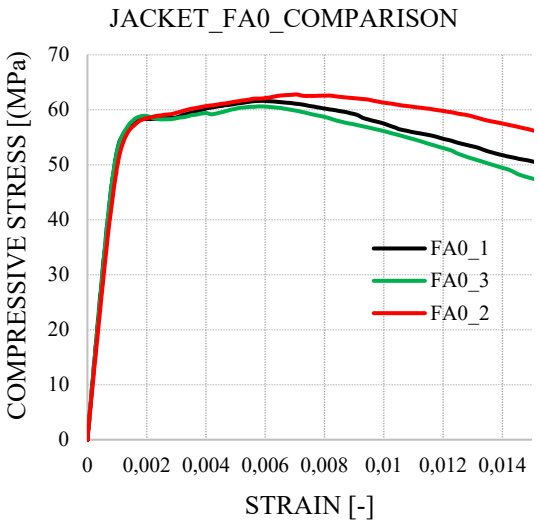

Figure 6.12 – FA0 Curves comparison.

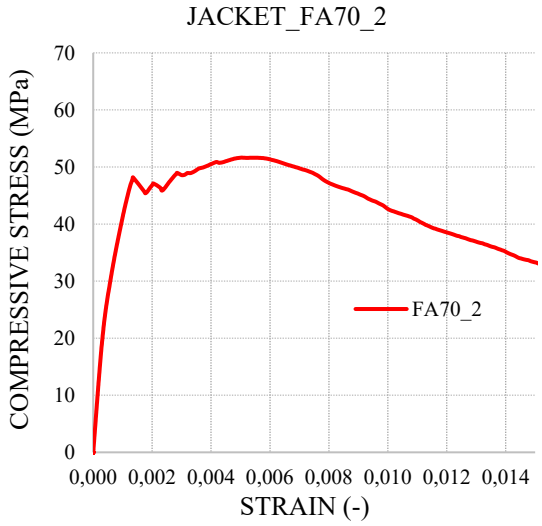

Figure 6.13 – Stress-strain curves: jacket FA70_2.

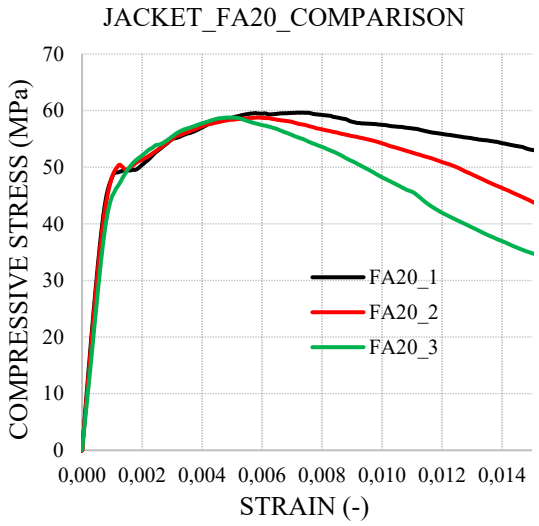

Figure 6.14 – FA20 Curves comparison.

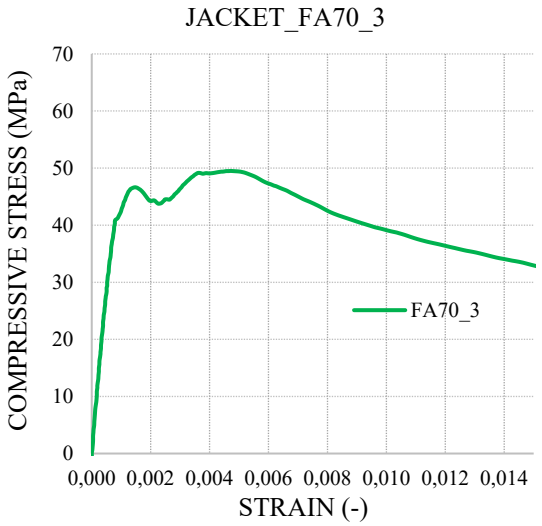

Figure 6.15 – Stress-strain curves: jacket FA70_3.

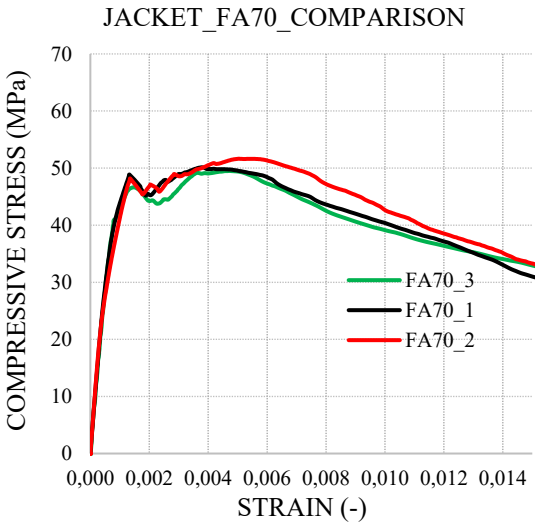

Figure 6.16 – FA70 Curves comparison.

Table 6.1 – Mechanical parameters of concrete cylinders not reinforced.

	SPECIMENS WITHOUT JACKETS								
	NAME	Max Load [kN]	Max Load [MPa]	Deformation associated [-]	Pmax/3 [kN]	εl (P/3) [-]	εv (P/3) [-]	Poisson's Ratio ν [-]	Ecm [GPa]
NC_CORE	NC_1	362.00	46.09	0.0026	120.67	0.000089	0.00046	0.19	34.79
	NC_2	346.70	44.14	0.0028	115.57	0.000096	0.00045	0.21	34.35
	NC_3	366.00	46.60	0.0025	122.00	0.000089	0.00049	0.18	34.91
	NC_4	341.20	43.44	0.0023	113.73	0.000087	0.00046	0.19	34.18

Table 6.2 – Mechanical parameters of concrete cylinders reinforced with UHP-FRCC jackets.

`	SPECIMENS WITH JACKETS								
	TYPE OF JACKETING	Max Load [kN]	Max Load [MPa]	Deformation associated [-]	Pmax/3 [kN]	εl (P/3) [-]	εv (P/3) [-]	Poisson's Ratio ν [-]	Ecm [GPa]
FA0	FA0_1	484.00	61.62	0.0058	161.33	0.000063	0.000333	0.19	37.96
	FA0_2	493.20	62.80	0.0071	164.40	0.000079	0.000380	0.21	38.18
	FA0_3	476.00	60.61	0.0057	158.67	0.000061	0.000336	0.18	37.77
FA20	FA20_1	468.40	59.64	0.0072	156.13	0.000058	0.000303	0.19	37.59
	FA20_2	461.60	58.77	0.0058	153.87	0.000058	0.000316	0.18	37.43
	FA20_3	461.60	58.77	0.0048	153.87	0.000059	0.000366	0.16	37.43
FA70	FA70_1	393.80	50.14	0.0038	131.27	0.000056	0.000262	0.21	35.68
	FA70_2	405.60	51.64	0.0050	135.20	0.000058	0.000261	0.22	36.00
	FA70_3	388.80	49.50	0.0049	129.60	0.000065	0.000303	0.21	35.55

Annex 3

4-Point Bending Test

- FIRST SERIES -12 beams

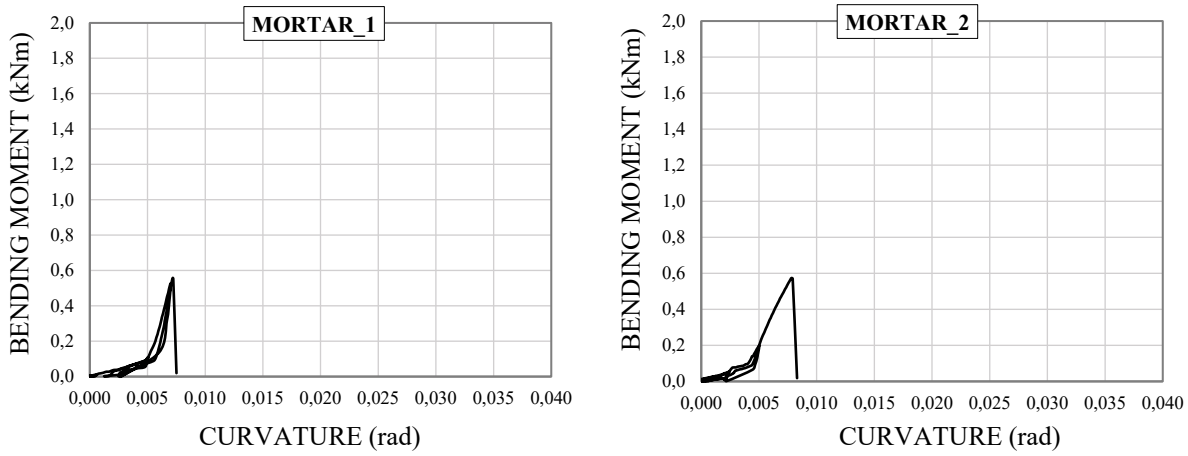

Figure 7.1 – Moment-Curvature curves of plain mortar beams (specimens 1-2).

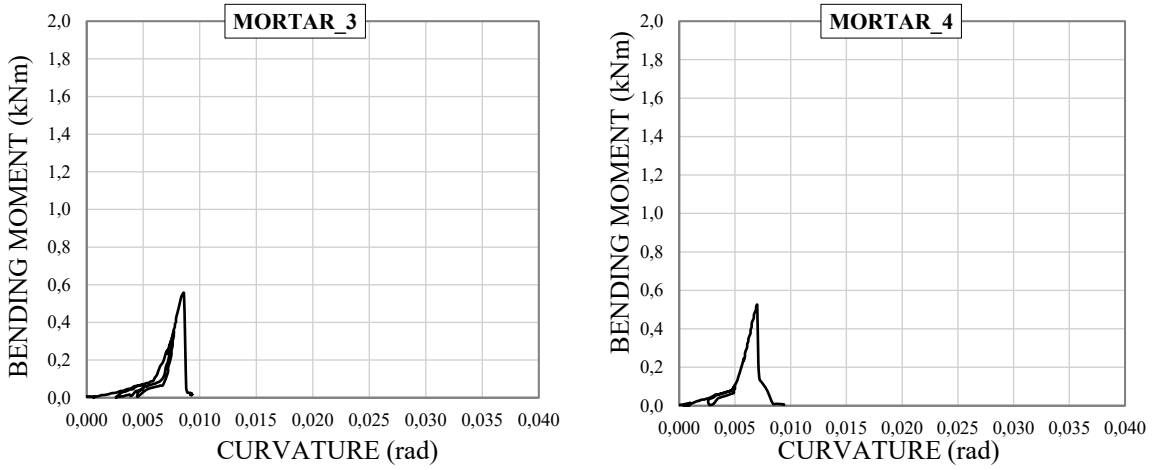

Figure 7.2 – Moment-Curvature curves of plain mortar beams (specimens 3-4).

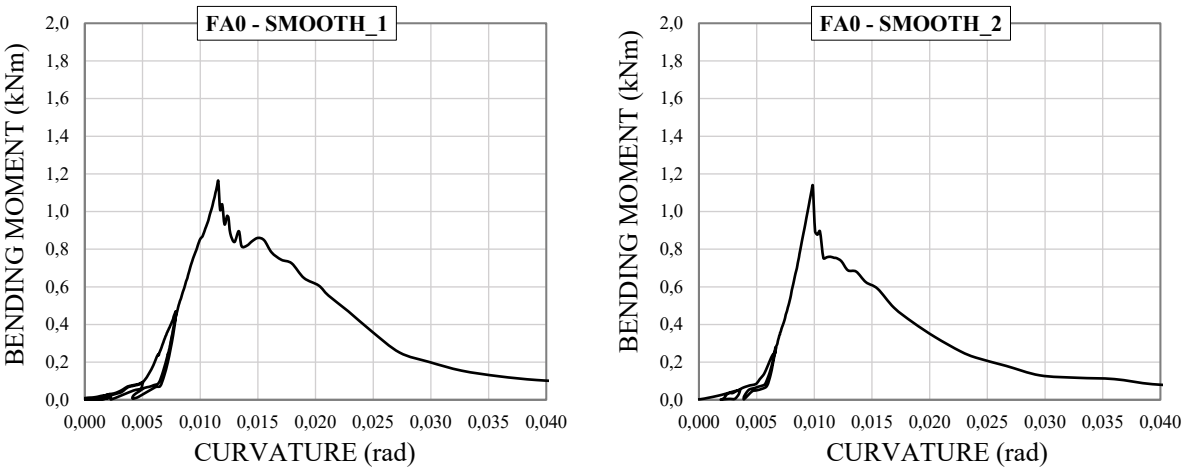

Figure 7.3 – Moment-Curvature curves of beams reinforced by smooth UHP-FRCC plate (FA0).

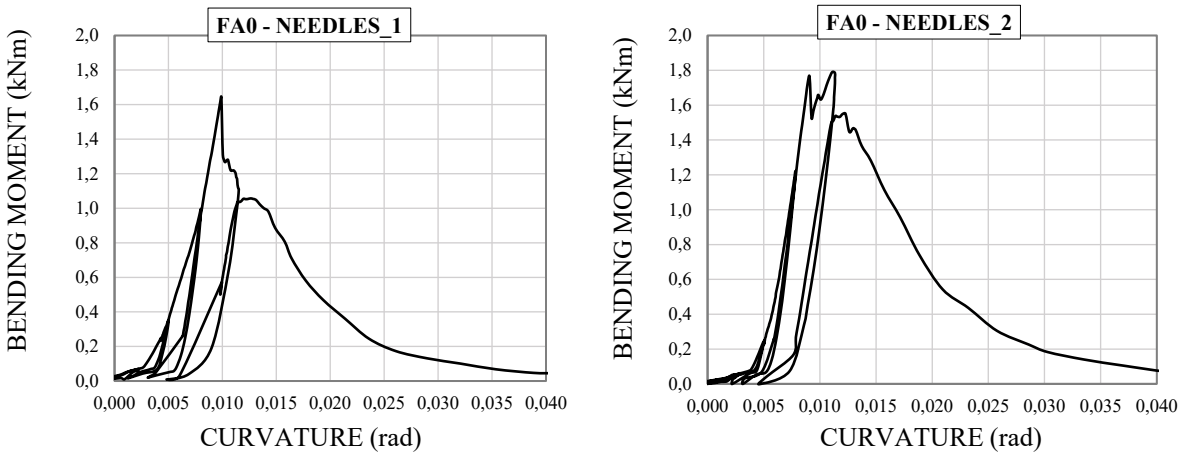

Figure 7.4 – Moment-Curvature curves of beams reinforced by UHP-FRCC plate with needles (FA0).

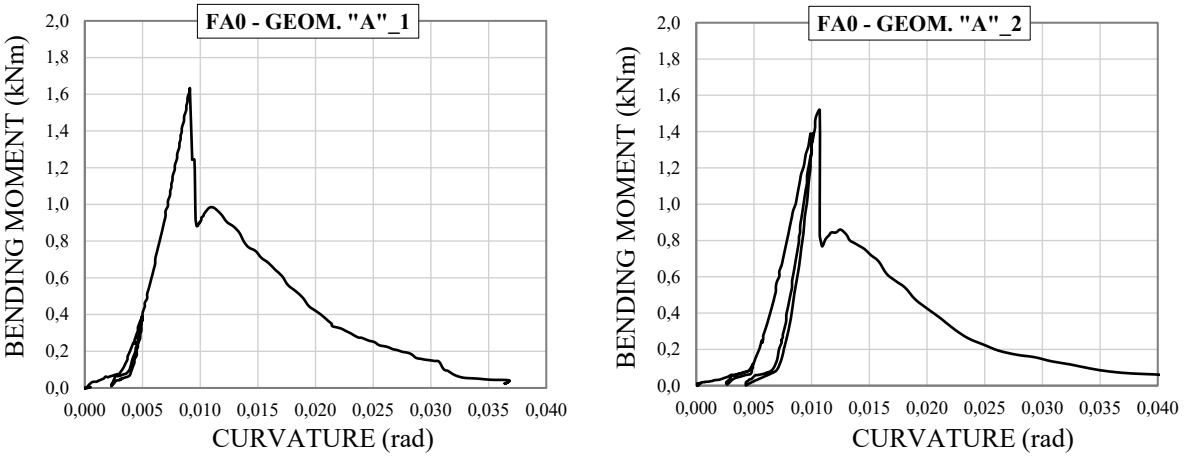

Figure 7.5 – Moment-Curvature curves of beams reinforced by UHP-FRCC layer with Geom. "A" (FA0).

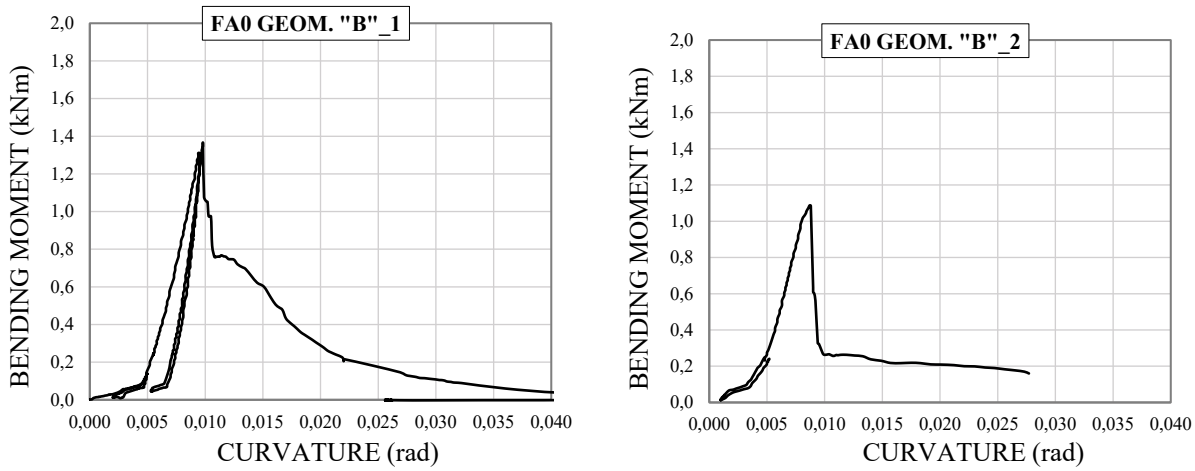

Figure 7.6 – Moment-Curvature curves of beams reinforced by UHP-FRCC layer with Geom. "B" (FA0).

- SECOND SERIES - 14 beams + 4 beams with UHP-FRCC layer and steel bars

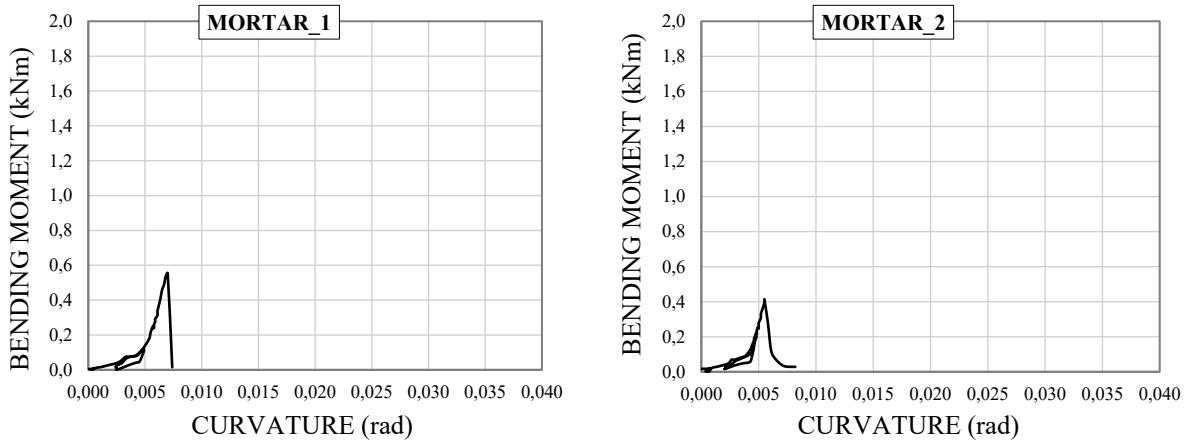

Figure 7.7 – Moment-Curvature curves of plain mortar beams.

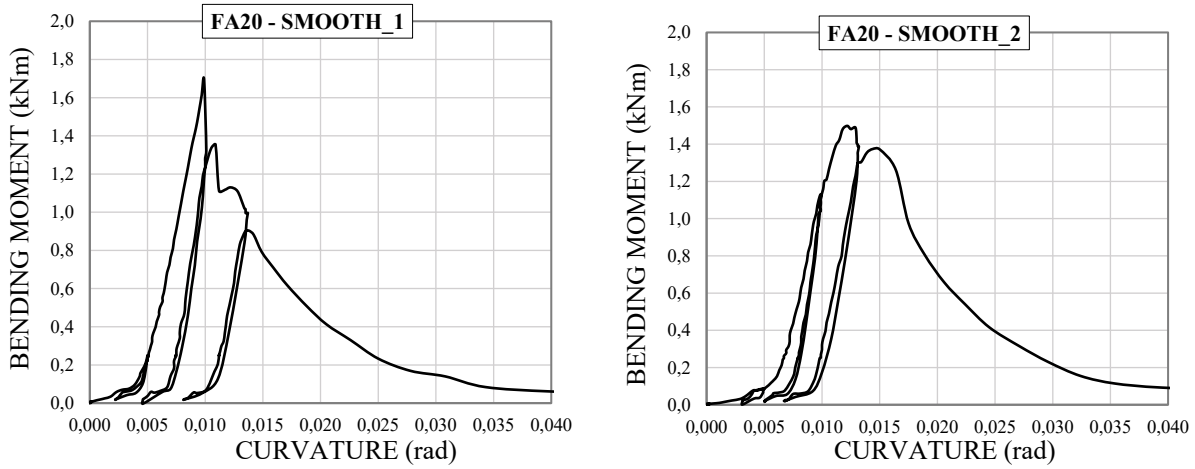

Figure 7.8 – Moment-Curvature curves of beams reinforced by smooth UHP-FRCC plate (FA20).

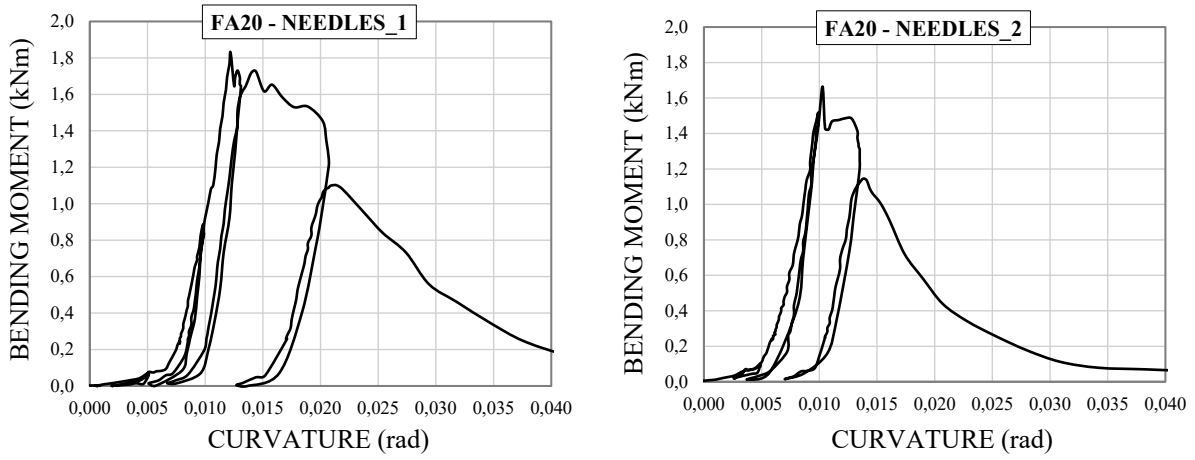

Figure 7.9 – Moment-Curvature curves of beams reinforced by UHP-FRCC plate with needles (FA20).

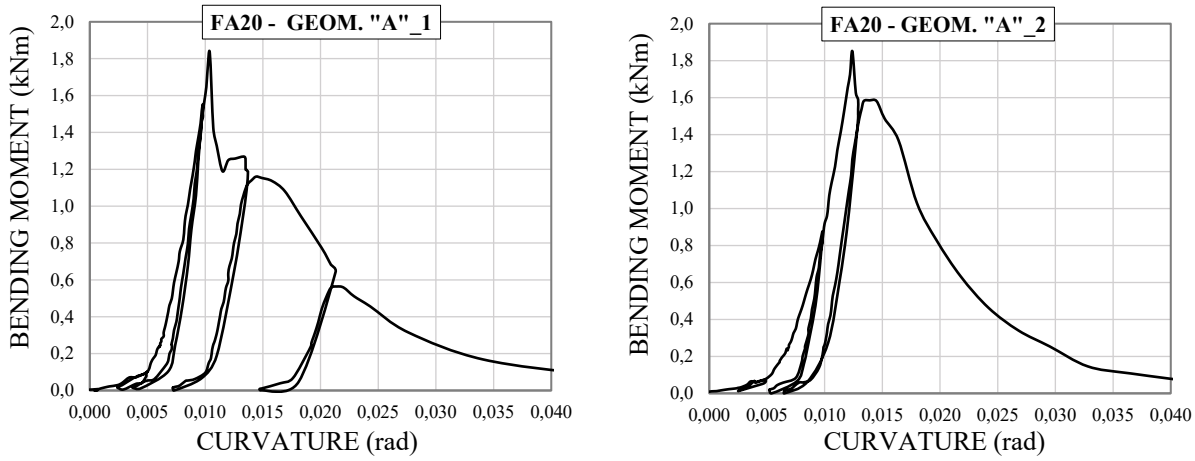

Figure 7.10 – Moment-Curvature curves of beams reinforced by UHP-FRCC layer with Geom. "A" (FA20).

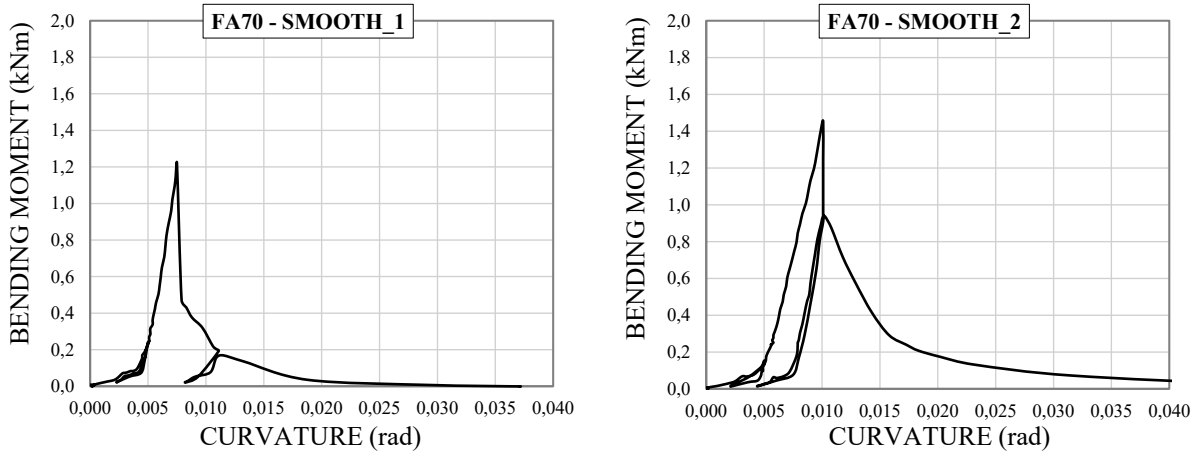

Figure 7.11 – Moment-Curvature curves of beams reinforced by UHP-FRCC plate with needles (FA70).

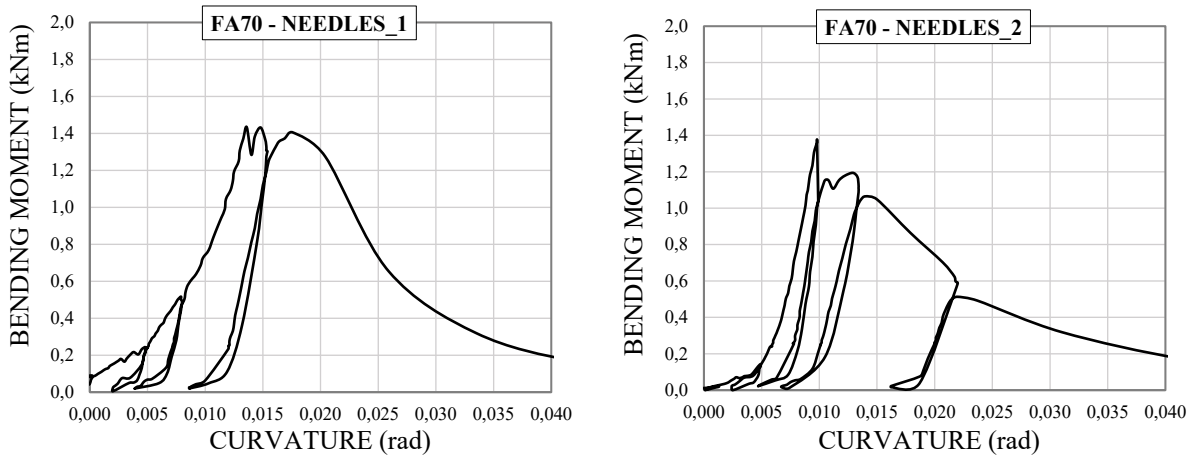

Figure 7.12 – Moment-Curvature curves of beams reinforced by UHP-FRCC plate with needles (FA70).

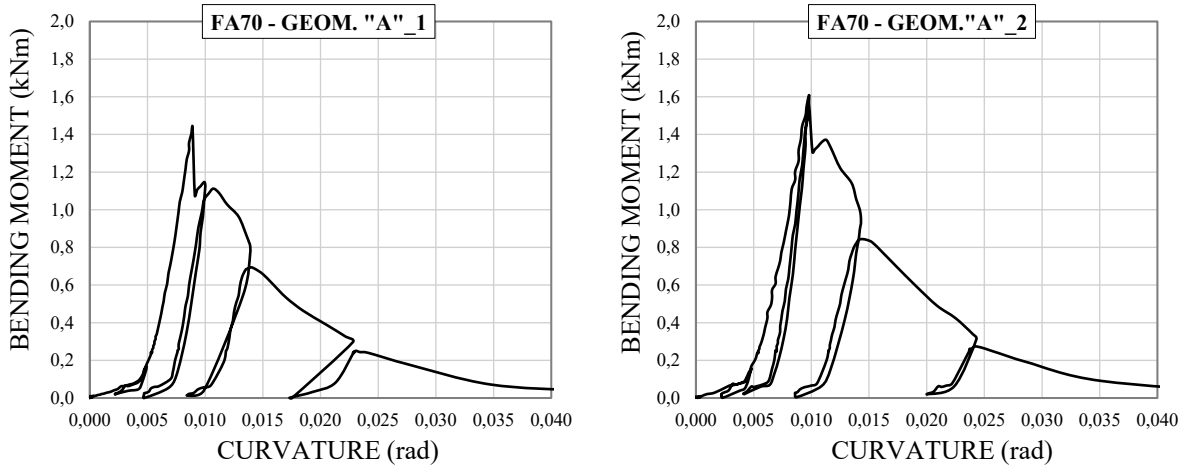

Figure 7.13 – Moment-Curvature curves of beams reinforced by UHP-FRCC layer with Geom. "A" (FA70).

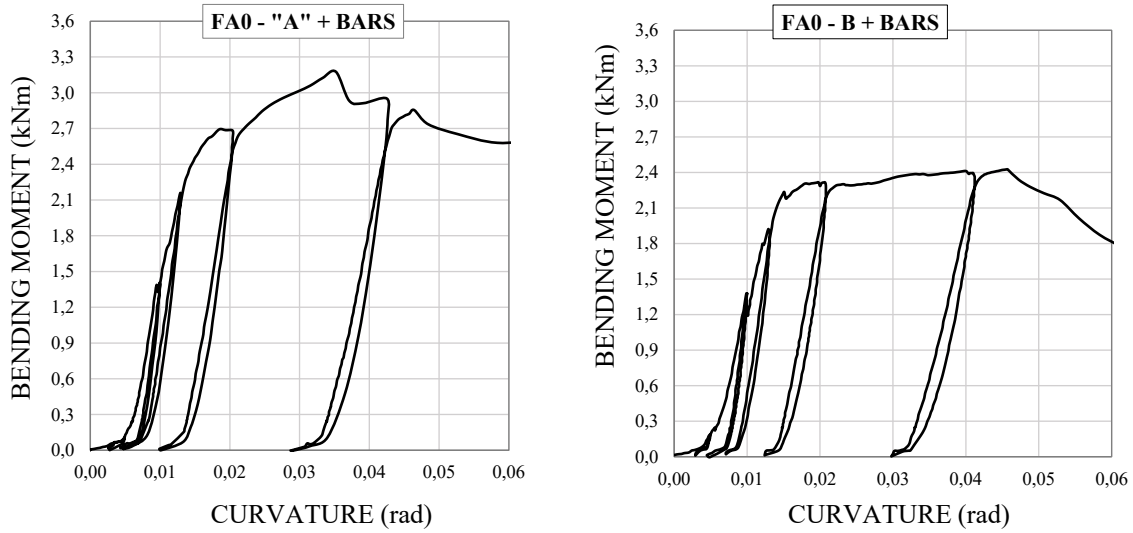

Figure 7.14 – Moment-Curvature curves of beams reinforced by UHP-FRCC layer and steel bars (FA0 - "A", FA0 - "B").

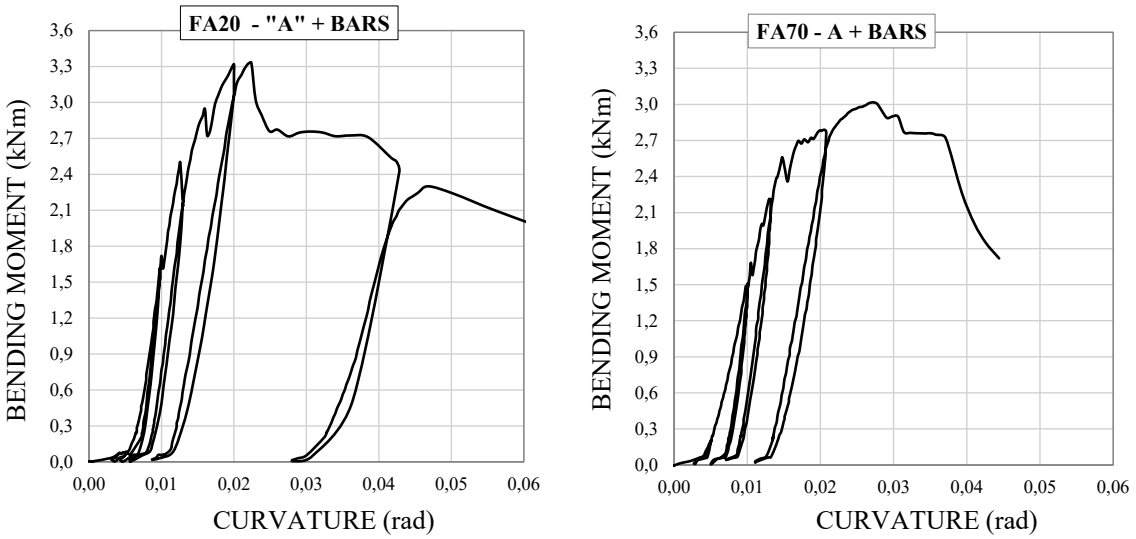

Figure 7.15 – Moment-Curvature curves of beams reinforced by UHP-FRCC layer - geom. "A" and steel bars (FA20, FA70).

Table 7.1 –Flexural resistances obtained during the experimental investigation (average values).

MIXTURE	TYPE OF REINFORCEMENT	MAX LOAD (kN)	MAX BENDING MOMENT (kNm)
MORTAR + FA0	SMOOTH	23.00	1.15
	GEOM. A	31.51	1.58
	GEOM. B	27.34	1.37
	NEEDLES	34.34	1.72
	GEOM. A + BARS	63.52	3.18
	GEOM. B + BARS	48.54	2.43
MORTAR + FA20	SMOOTH	31.94	1.60
	GEOM. A	36.82	1.84
	NEEDLES	34.91	1.75
	GEOM. A + BARS	66.62	3.33
MORTAR + FA70	SMOOTH	26.72	1.34
	GEOM. A	30.50	1.53
	NEEDLES	28.12	1.41
	GEOM. A + BARS	60.32	3.02
PLAIN MORTAR	PLAIN MORTAR	10.61	0.53

REFERENCES

[1] Fantilli, A.P., and Chiaia, B., "The work of fracture in the eco-mechanical performances of structural concrete," in *Journal of Advanced Concrete Technology*, v. 11, pp. 282-290, 2013

[2] Wille, K., El-Tawil, S., and Naaman, A.E., "Properties of strain hardening ultra high performance fiber reinforced concrete (UHP-FRC) under direct tensile loading", in *Cement & Concrete Composites*, v. 48, pp.53–66, 2014

[3] Herold, G., and Muller, H.S., "Measurement of porosity of Ultra High Strength Fibre Reinforced Concrete," in *Proceedings of the International Symposium on Ultra High Performance Concrete,* pp. 685-694, 2014

[4] Naaman, A.E., "High performance fiber reinforced cement composites: classification and applications*",* in *International Workshop "Cement Based Materials and Civil Infrastructure (CBM-CI),* Karachi, Pakistan, pp. 389-401, 2007

[5] Naaman, A.E., "High Performance Fiber Reinforced Cement Composites", in Shi, C., Mo, Y.L., *High-Performance Construction Materials: science and applications*, Singapore, pp. 91-153, 2008

[6] Bache, H.H., "Densified cement/ultrafine particle-based materials", in *Second International Conferences on Superplasticizers on Concrete*, Ottawa, ON, Canada, pp. 25-32, 1981

[7] Bache, H.H., "Compact reinforced composite basic principles", *CBL Report*, n. 41, Aalborg, Denmark, 1987

[8] Bache, H.H., "The new strong cements: their uses in structures", in *Physics in Technology*, v.19, n.2, Aalborg's Portland Cement and Concrete Laboratory, Aalborg, Denmark, pp. 43-50, 1988

[9] Kendall, A. J. Howard, and J. D. Birchall, "The relation between porosity, microstructure and strength, and the approach to advanced cement-based materials", in *Philosophical Transactions of the Royal Society of London,* Series A, Mathematical and Physical Sciences, v. 310, n. 1511, London, England, pp. 139-153, 1983

[10] Rossi, P., Acker, P., and Malier, Y., "Effect of steel fibres at two stages: the material and the structure", in *Materials and Structures*, v. 20, pp. 436-439, 1987

[11] Rossi, P., "Les bétons de fibres métalliques", *Presses de L'ENPC*, 1998

[12] Rossi, P., "Ultra-High Performance Fibre Reinforced Concretes (UHPFRC): An overview", in *Proceedings of the Fifth International RILEM Symposium on Fibre-Reinforced Concretes*, Lyon, France, pp. 87-100, 2000

[13] Gambarova, P.G., "Overview of recent advancements in FRC knowledge and applications, with specific reference to high temperature", in *Proceedings of the Sixth International RILEM Symposium on Fibre-Reinforced Concretes*, Varenna, Italy, pp. 125-140, 2004

[14] Markovic, I., Walraven, J.C., and M. van Mier, J.G., "Experimental evaluation of fibre pullout from plain and fibre reinforced concrete", in *International Workshop High Performance Fiber Reinforced Cement Composites*, RILEM Publications SARL, Cachan, France, pp. 429-438, 2003

[15] Brand, R., Pulles, T., Van Gijlswijk, R., Fribourg-Blanc, B., and Courbet, C., "European pollutant emission register. Final report", European Commission, 2004

[16] Bernstein, L., J Roy, K.C., Delhotal, J., Harnisch, R., Matsuhashi, L., Price, K., et al., "Climate Change 2007: Synthesis Report", in *Contribution of Working Groups I, II and III to the Fourth Assessment Report of the Intergovernmental Panel on Climate Change, IPCC 2007*, Geneva, Switzerland, pp. 104, 2007

[17] Parrott, L., "Cement, concrete and sustainability. A report on the progress of the UK cement and concrete industry towards sustainability", British Cement Association, 2002

[18] Teller, P.H., Denis, S., Renzoni, R., Germain, A., Delaisse, P.H., D'inverno, H., "Use of LCI for the decision-making of a Belgian cement producer: a common methodology for accounting CO_2 emissions related to the cement life cycle", in *Eighth LCA case studies symposium SETAC-Europe*, 2000

[19] Habert, G., and Roussel, N., "Study of two concrete mix-design strategies to reach carbon mitigation objectives", *Cement & Concrete Composites*, v. 31, pp 397–402, 2009

[20] Turner, L.K., and Collins, F.G., "Carbon dioxide equivalent (CO_2-e) emissions: A comparison between geopolymer and OPC cement concrete", *Construction and Building Materials*, v. 43, pp. 125-130, 2013

[21] Stengel, T., Reger, J., and Heinze, D., "Life Cycle Assessment of Geopolymer Concrete - what is the environmental benefit?", In *Proceedings Concrete 09, 24th Biennial Conf. Australia Concrete Institute, Sydney, Concrete Institute of Australia*, pp. 54-62, 2009

[22] Mehta, P.K., and Monteiro, P.J.N., *Concrete – microstructure, properties, and materials*, 4 ed., New York, McGraw-Hill, 2014

[23] Dragas, J., Marinković, S., Ignjatovic, I., and Tosic, N., "Properties of high-volume fly ash concrete and its role in sustainable development", in *Journal of Faculty of Civil Engineering*, Conference: International Conference Contemporary Achievements in Civil Engineering Subotica, Serbia, April 2014, pp. 849-858, 2014

[24] Bilodeau, A., and Malhotra, V.M., "High-Volume Fly Ash System: Concrete Solution for Sustainable Development", *ACI Materials Journal*, v. 97, n.1, American Concrete Institute, pp. 41-48, 2000

[25] Holman, K.R., Volz, J.S., and Myers, J.J., "Comparative Study on the Mechanical and Durability Behavior of High-Volume Fly Ash Concrete versus Conventional Concrete", in *First International Conference on Concrete Sustainability (ICCS 2013)*, 2013

[26] Aghdasi, P., Heid, A.E., and Chao, Shih-Ho, "Developing Ultra-High-Performance Fiber-Reinforced Concrete for Large-Scale Structural Applications", *ACI Materials Journal*, v. 113, pp. 559-570, 2016

[27] Nishiwaki, T., Suzuki, K., et al., "Ecological and Mechanical Properties of Ultra High Performance – Fiber Reinforced Cementitious Composites Containing High Volume Fly Ash", in Mechtcherine V., Slowik V., Kabele P. (eds), *Strain-Hardening Cement-Based Composites*, SHCC 2017, RILEM Bookseries, v. 15, Springer, Dordrecht, 2018

[28] Longo, M., "The behavior of concrete confined by ultra high performance – fiber reinforced cementitious composite", *Final report for Colabs project*, Life cycle engineering laboratory, Tohoku University, Sendai, Japan, pp. 16-18, 2017

[29] Mander, J.B., Priestley, M.J.N., and Park, R., "Theoretical stress-strain model for confined concrete", in *Journal of Structural Engineering*, ASCE, v. 114, n. 8, pp. 1804-1826, 1988

[30] Binici, B., "An analitycal model for stress-strain behavior of confined concrete", Engineering Structures, v. 27, pp. 1040-1051, 2005

[31] Sargin, M., "Stress-strain relationships for concrete and the analysis of structural concrete sections", Solid Mechanics Division, University of Waterloo, Canada, 1971

[32] Sargin, M., Ghosh, S., and Handa, V.K., "Effects of lateral reinforcement upon the strength and deformation properties of concrete", in *Magazine of Concrete Research,* v. 23, issue 75-76, pp. 99-110, 1971

WEBSITES CITATIONS

[33] Balasaheb, E.Gite, Madhuri, K. Rathi, Rajesh, S.Rajguru, Asif, P.Shaikh Amrutvahini, "Advance Construction Material – Micro Silica in Concrete", posted in *Concrete Engineering, Research Papers,* www.engineeringcivil.com, https://www.engineeringcivil.com/advance-construction-material-micro-silica-in-concrete.html

[34] "Concrete Testing - Concrete Cubes Testing Service Provider from Chennai", www.indiamart.com, https://www.indiamart.com/company/6379072/concrete-testing.html

[35] "FLY ASH CONCRETE AND ICFS", in *The Insulating Concrete Forms Magazine*, www.icfmag.com, 2014. https://www.icfmag.com/2014/11/fly-ash-concrete-and-icfs/

[36] "Lavorabilità del calcestruzzo", Gruppo Gatti S.P.A., www.gruppogattispa.it, http://www.gruppogattispa.it/prodotti.php?DOC_INST=12

[37] "Flow table", www.rex-rental.jp, https://www.rex-rental.jp/nco/c-206.html

[38] "The diameter is measured and compared with the starting diameter", Image 18 of 34, University of Kentucky, www.caer.uky.edu, http://www.caer.uky.edu/kyasheducation/testing-mortar.shtml

[39] "Gilson Concrete Air Meter w/ Stainless Steel Gauge", www.globalgilson.com, https://www.globalgilson.com/concrete-air-meter

[40] "Compressometer-Extensometer", UTEST Material Testing Equipment, www.utest.com.tr, http://www.utest.com.tr/en/23425/Compressometer-Extensometer

[41] "Strain gauges", KYOWA, www.kyowa-ei.com, http://www.kyowa-ei.com/eng/product/category/strain_gages/index.html

REGULATIONS

[42] ASTM C 143/C 143M – 03, "Standard Test Method for Slump of Hydraulic-Cement Concrete", 2003

[43] ASTM C1437 – 07, "Standard Test Method for Flow of Hydraulic Cement Mortar", 2007

[44] ASTM C230/C230 M – 08, "Standard Specification for Flow Table for Use in Tests of Hydraulic Cement", 2008

[45] ASTM C 109/C 109M – 07, "Standard Test Method for Compressive Strength of Hydraulic Cement Mortars (Using 2-in. or [50-mm] Cube Specimens)", 2007

[46] ASTM C231 – 03, "Standard Test Method for Air Content of Freshly Mixed Concrete by the Pressure Method", 2003

[47] JIS A 1106:2006, "Method of test for flexural strength of concrete", STANDARD by Japanese Industrial Standard / Japanese Standards Association, 2006

[48] JCI-S-003-2007,"Method of test for bending moment–curvature curve of fiber-reinforced cementitious composites", Japan Concrete Institute Standard, 2007

[49] JIS A 1149:2017, "Method of test for static modulus of elasticity of concrete", STANDARD by Japanese Industrial Standard / Japanese Standards Association, 2017

Acknowledgements

To conclude, I would like to reiterate my gratitude to all those who have contributed to this academic achievement. Therefore, I want to thank first my parents and my brothers, who have consistently supported and encouraged me to always do my best.
Special mention should go to Sara, who has been ever by my side during these years.
I wish to thank prof. Alessandro Pasquale Fantilli, my tutor, for his willingness and kindness in supervising my research study during the thesis.
Special thank goes to prof. Tomoya Nishiwaki, for giving me the opportunity to spend a period at the Tohoku University. He was an excellent professional example for everything I learnt from him and I am so proud to have worked in his team at the Department of Architecture and Building Science in Sendai (Japan).
Lastly, I am thankful all those who, among colleagues and friends, with their collaboration and patience have helped me, sharing together the entire academic path.
To you all THANK YOU!

Valerio